UNIVERSITY OF OKLAHOMA

GRADUATE COLLEGE

STRUCTURE-INDEPENDENT CONFORMAL QUASI-ISOTROPIC ANTENNAS FOR SMALL UNMANNED AIRCRAFT SYSTEM APPLICATIONS

A THESIS

SUBMITTED TO THE GRADUATE FACULTY

in partial fulfillment of the requirements for the

Degree of

MASTER OF SCIENCE

By

TAYLOR ANDREW POYDENCE

Norman, Oklahoma

2017

STRUCTURE-INDEPENDENT CONFORMAL QUASI-ISOTROPIC ANTENNAS FOR SMALL UNMANNED AIRCRAFT SYSTEM APPLICATIONS

A THESIS APPROVED FOR THE
SCHOOL OF ELECTRICAL AND COMPUTER ENGINEERING

BY

Dr. Jessica Ruyle, Chair

Dr. Caleb Fulton

Dr. Phillip Chilson

Table of Contents

List of Tables vi

List of Figures vii

Abstract xi

1 Introduction 1
- 1.1 Motivation . . . 1
- 1.2 Thesis Outline . . . 3

2 Review of SUAS Antenna Structures 4
- 2.1 Introduction . . . 4
- 2.2 Rubber Duck Antennas . . . 5
- 2.3 Cloverleaf Antennas . . . 6
- 2.4 Brief Survey of Conformal and Quasi-Isotropic Antennas . . . 9
- 2.5 Summary . . . 10

3 Adapted Historical Omnidirectional Antennas 12
- 3.1 Introduction . . . 12
- 3.2 Impedance Modified Loop Antennas . . . 13
  - 3.2.1 Introduction . . . 13
  - 3.2.2 Design and Theory . . . 13
  - 3.2.3 Measurements and Integration of Chip Baluns . . . 18
  - 3.2.4 Investigation of Optimal Placement . . . 21
  - 3.2.5 Alternative Loading Schemes . . . 24
- 3.3 Modified Crossed Dipole Antennas . . . 26
  - 3.3.1 Introduction . . . 26
  - 3.3.2 Design and Theory . . . 27
- 3.4 Conclusions . . . 31

4 Curved Folded Dipole Antenna 33
- 4.1 Introduction . . . 33
- 4.2 Design and Theory . . . 34
- 4.3 Antenna Performance Flexibility . . . 40

4.4 Measurements 45
4.5 Investigation of Optimal Placement 48
4.6 Modifications for Conductive Backing 52
4.7 Conclusions 56

5 Flight Measurements **58**
5.1 Introduction and Goals 58
5.2 Fixed Wing Flight Tests 59
5.3 Quadrotor Tests 60
5.3.1 Power Transfer and BER 61
5.3.2 Multi-Metric Assessment with SDR 66
5.3.3 Conclusions 67

6 Conclusions and Future Work **69**
6.1 Conclusions 69

References **74**

List of Tables

3.1 Inductor-Loaded Cross Dipole Antenna Parameters 30

4.1 Peak Real Impedance and Radiation Efficiency Trends for In-Plane Curvature in Air and on 10mil Rogers 5880 Substrate at resonant frequency 35
4.2 Impedance and Radiation Efficiency Trends with Conformation . . . 40
4.3 Size of CFDA variations resulting from increasing bandwidth through varying the line widths and decreasing the angle of curvature to compensate for impedance changes 44

5.1 In-flight performance results for the 50Ω loaded loop antenna on the University of Kentucky fixed-wing aircraft 60
5.2 Communication metrics generated from telemetry data from flying the IRIS craft to 100 meters with antennas positioned standalone from the airframe 64
5.3 Communication metrics generated from telemetry data from flying the IRIS craft to 300 meters with antennas positioned conformal to the structure, wrapping slightly about the top of the front end 66

List of Figures

1.1 Antenna configuration of the included coiled monopole rubber duck antenna on the IRIS craft used as an antenna test platform 2

2.1 Measured radiation patterns for rubber duck antennas implemented with a half-wave dipole (black) and a coil loaded electrically small whip (red) 6
2.2 Cloverleaf antenna geometries: 3 element (left) and 5 element (right) 7
2.3 Far-field realized gain of the 3-element cloverleaf antenna 8
2.4 Far-field realized gain of 3-element and 5-element cloverleaf antennas emphasizing similarity to a dipole and slightly higher consistency of the 5-element antenna in the H-plane 8
2.5 Example of perpendicularly bent monopole structure used to distribute currents strategically for generation of a quasi-isotropic pattern 10

3.1 Geometry and design parameters of the nominal impedance modified loop antenna 15
3.2 Input resistance trends for varying % fill of the patch in the impedance modified loop at the corresponding resonance for each respective value of d_1 16
3.3 Fabricated Loop antennas: 2.4 GHz 50 Ω diamond loop (left), 915 MHz 50 Ω rectangular loop (top), and 915 MHz 100 Ω rectangular loop with 2:1 chip balun (bottom) 19
3.4 Simulated and measured results for the fabricated rectangular loops 20
3.5 Measured versus simulated Azimuth (left) and Elevation (right) radiation patterns for rectangular 50 Ω loop 21
3.6 Simulated rectangular loop with a lumped port excitation and measured rectangular loop with a 1:1 high inductance (18 μH) chip balun 22
3.7 Conformally mounted impedance modified loop antenna in the top (left), rear (middle), and bottom (right) positions as mentioned . . . 23
3.8 Radiation pattern E-Planes (left) and H-Planes (right) of 100 Ω loop with 2:1 balun conformally attached to IRIS aircraft in top, bottom, and rear locations showing impact of placement on antenna functionality 23

3.9 Insertion loss of 100 Ω loop with 2:1 balun conformally attached to IRIS aircraft in top, bottom, and rear locations showing impact of placement on antenna functionality 24
3.10 Battery and dielectric loaded loop antenna geometry (left) and simulation results (right) 25
3.11 Full radiation pattern (left) and perpendicular elevation plane patterns (right) for simulated battery and dielectric loaded loop antenna in dBi 25
3.12 Measured insertion loss of the craft internals loaded impedance modified loop antenna in its intended position on the bottom of the craft and an alternate position on the top center of the craft 27
3.13 Progression of linear crossed dipoles into meander-line loaded crossed dipoles and corresponding electrical size of minimal square package at each stage 28
3.14 Reflection coefficient magnitude for the discussed stages of development for the modified crossed dipole antenna structure 29
3.15 Simulated radiation pattern for the modified crossed dipoles implemented with helical wire inductor loads (left) and planar meander line inductor loads (right) 30

4.1 Geometry and design parameters for the curved folded dipole antenna in the nominal equal width configuration (left) and a wideband configuration (right) 35
4.2 Reflection coefficient for selected angles of curvature for a 915 MHz design with a 50 Ω feed port in HFSS 36
4.3 Depiction of the E-Plane and H-Plane for far field radiation for the CFDA with both planes referenced in angle to the symmetry line of the radiator geometry 37
4.4 Progression of radiation pattern with increasing angle of curvature in the E-Plane (left) and in the H-Plane of the unconformed antenna (right) 37
4.5 E-Plane radiation pattern comparison for the segmented currents numerical model and simulation with 180 degree (left) and 135 degree (right) angles of curvature 38
4.6 Depiction of the conformal angle at ϕ = 60° (left) and the half-cylindrical bending geometry with a conformal angle ϕ = 90° (right) 40
4.7 Reflection coefficient for discrete conformation angles for a 915MHz design 41
4.8 Comparison of CFDA impedance variations projected by conventional folded dipole impedance scaling to simulations, resulting from adjusting w_2 with d =3mm, w_1 =1mm, and $\theta = 176°$ 42

4.9 Impedance progression of the CFDA as w_2 is increased and θ is decreased to create offsetting impedance changes and achieve increased bandwidth 43
4.10 Radiation pattern progression of the CFDA as w_2 is increased and θ is decreased to incur offsetting impedance changes and achieve increased bandwidth 44
4.11 Fabricated 915 MHz nominal CFDA with bazooka balun (top), 915 MHz wideband CFDA (left), and example 2.4 GHz CFDA (right) . 46
4.12 Simulated and measured results for the fabricated nominal and wideband CFDA variations 47
4.13 Measured versus simulated H-Plane (left) and E-Plane (right) radiation patterns for thin nominal quasi-isotropic CFDA 47
4.14 Measured versus simulated H-Plane (left) and E-Plane (right) radiation patterns for wideband variation of the CFDA 48
4.15 E-Plane radiation pattern comparison for the segmented currents numerical model and measurements of the nominal CFDA design (left) and the wideband design (right) 48
4.16 Conformally mounted 20MHz bandwidth CFDA variation in the top (left), rear (middle), and bottom (right) positions as mentioned . 50
4.17 Radiation pattern E-Planes (left) and H-Planes (right) of 20 MHz nominal CFDA conformally attached to IRIS aircraft in top, bottom, and rear locations showing impact of placement on antenna functionality 50
4.18 Insertion loss of nominal 20 MHz bandwidth CFDA conformally attached to IRIS aircraft in top, bottom, and rear locations showing impact of placement on antenna functionality 51
4.19 Conformally mounted 20MHz bandwidth CFDA variation in the top (left), rear (middle), and bottom (right) positions as mentioned . 52
4.20 Radiation pattern E-Planes (left) and H-Planes (right) of 80 MHz nominal CFDA conformally attached to IRIS aircraft in top, bottom, and rear locations showing impact of placement on antenna functionality 52
4.21 Insertion loss of nominal 20 MHz bandwidth CFDA conformally attached to IRIS aircraft in top, bottom, and rear locations showing impact of placement on antenna functionality 53
4.22 Comparison of CFDA impedance variations projected by conventional folded dipole impedance scaling to simulations, resulting from adding additional radiating elements to the folded dipole structure . 54
4.23 Close-up geometry of the 7-line CFDA implemented on a full-wavelength square 10 mil substrate with a ground plane 3mm below 56

5.1 Perpendicular conformal implementation of loaded loop antennas adhered to University of Kentucky styrofoam fixed-wing aircraft with masking tape 59
5.2 Quadrotor test configuration for antennas in both conformal (left) and non-conformal (right) configurations on the IRIS aircraft 61
5.3 CFDA radiation pattern measurements depicting substantial variation from simulation and air measurement when adhered to craft with 3mm thick Velcro 62
5.4 Impedance modified loop radiation pattern measurements depicting substantial variation from simulation and air measurement when adhered to craft with 3mm thick Velcro 63
5.5 Example antenna configurations for base station telemetry module and for IRIS aircraft with both conformal (left) and non-conformal (right) positioning on the aircraft 64

Abstract

Communication systems for aircraft are often implemented through antennas that protrude from the airframe and contain radiation nulls - which have detrimental effects on the aerodynamics of the craft and its ability to maintain a strong data link with a ground station through maneuvers, respectively. Small Unmanned Aircraft Systems (SUAS) in particular would greatly benefit from the use of quasi-isotropic and conformal antennas due to the increased impact of aerodynamics and communication links on their performance. Previous work has pursued antennas that either produce an approximately uniform power distribution or function favorably under significant conformation. This work provides an investigation of antennas that exhibit traits of conformality or quasi-isotropic radiation when conformed to a SUAS airframe. A specific variant of a dipole structure is explored and shown to have a highly quasi-isotropic radiation pattern within a size constrained form factor and conformal to the surface of typical SUAS. Considerations are made for the practical challenges of conformal attachment to SUAS and the tangible improvement on the communication system is assessed.

Chapter 1

Introduction

1.1 Motivation

Development of antennas for Small Unmanned Aircraft Systems (SUAS) is a unique challenge due the extremely size-constrained form factors and airframe shapes that limit the geometry of the antenna that can be used. These constraints place fundamental limits on the performance of typical antenna structures that might be implemented [1]–[3]. Rubber duck antennas, favored for their small electrical size of the coiled monopole variety, are thus a widely used antenna structure for these applications where cost, size, and robustness are at a premium. Despite their ubiquity, these antennas suffer from radiation nulls, hindrance of craft aerodynamics, and often a considerable amount of loss with decreasing electrical size. Figure 1.1 exemplifies the potential design requirements made for an antenna that protrudes from the body of a craft. Antennas that are non-protrusive, planar, and more compact with improved performance are the primary concern of this work.

SUAS ideally need to maintain a constant communication link with the controller or ground station as they are remotely operated. This constant data link may generally be hard to maintain throughout flights as antennas do not radiate a signal uniformly in all directions [4]–[8]. SUAS systems must generally be prepared to

communicate in directions encompassing quite nearly the entire lower hemisphere relative to the craft. Additional considerations must be made if any degree of air-to-air communication is intended as well. Additionally, the SUAS in this investigation are tasked with real-time meteorological measurements throughout flight maneuvers. Thus a communication failure directly equates to data loss.

Figure 1.1: Antenna configuration of the included coiled monopole rubber duck antenna on the IRIS craft used as an antenna test platform

Previous work has attempted to approximate a uniform power distribution from an antenna to maintain a signal link regardless of orientation, and several designs have arisen approximating this result [1], [7], [8]. However, with the antenna designs that currently exist with as uniform a power distribution as possible, an emphasis has not been put on conformal applications or miniaturization. In this work we investigate antennas that are quasi-isotropic to attain a more stable data link despite the maneuvering of the SUAS and with minimal influence on the aerodynamics of the vehicle through their addition. As current antenna structures boast

simple, low-cost, and easy to implement designs, these traits are maintained as secondary goals in the development of the antennas herein.

1.2 Thesis Outline

The thesis begins by introducing the antenna structures prevalent in Small Unmanned Aircraft Systems and assesses the general disadvantages they may have for broad use in such applications. A brief survey of less commonplace novel and PCB-integrated structures is also included for consideration. This leads into Chapter 3 wherein adaptations of loop antennas and crossed dipole antennas are explored as improved conformal alternatives to the surveyed antennas. Chapter 4 explores an antenna structure in the form of a curved folded dipole which is conformal, quasi-isotropic, and performance flexible. Measurements of the radiation and RF communication performance for antennas on-board SUAS are discussed in Chapter 5 in an effort to quantify the tangible improvements the antennas discussed herein can make for relevant aerial communication systems. Chapter 6 covers the overall conclusions of the work, the larger implications of the results, and potential future direction that the research may take.

Chapter 2

Review of SUAS Antenna Structures

2.1 Introduction

Conventional antennas for SUAS applications typically fall in the category of electrically small portable antennas with omnidirectional radiation [9]. Omnidirectional in practice typically refers to equivalent radiation in one plane, generally in the the azimuth of the radiator, than isotropy. The most common type of antenna in this category is the rubber duck antenna as it can provide an omnidirectional pattern while having an electrical size less than a quarter wavelength. The skew planar antenna, first theorized by [10], has seen a recent resurgence as a popular antenna for SUAS applications due to its slightly increased beamwidth over a folded dipole and its offering of circular polarization, albeit at a much larger cost in physical size. Both antenna types provide quasi-omnidirectional radiation in the azimuthal plane but suffer from radiation nulls along their central axis [11][12]. These nulls make it difficult to maintain a data link at either a vertical or distant horizontal craft position with the antenna likewise oriented.

2.2 Rubber Duck Antennas

Rubber duck antennas have become ubiquitous for virtually every application that implements commercial off-the-shelf antenna structures. The term rubber duck generally refers to a largely variable class of wire dipoles and whips encased in a tight fitting rubberized casing or radome. Broadly lumped into the category of omnidirectional antennas, those which radiate equally well in all directions within a 2-D plane, these antennas may be viewed as one of the simplest to implement for basic radial communication. In practice, however, the generalization of the antenna class may obscure the fact that the various structural implementations can have vastly different RF characteristics even for identical design frequencies. In cases where a half-wave dipole is of a practical size, it is generally a preferable solution as the radiation pattern is well-defined and the efficiency is not hindered by electrical size reduction. Coil loaded whips have comparably more variable patterns due to the design variability of the coil used for loading the antenna and reducing the electrical size. At the lower GSM bands, this implementation of the rubber duck antenna merits further consideration due to its smaller size requirement. Figure 2.1 depicts the considerable measured variability in radiation pattern between a half wave dipole and coiled whip implementation for a 915 MHz rubber duck antenna that came standard with two different SUAS. Of particular note are the nulls in the H-Plane of the coiled whip rubber duck, the plane typically considered to be omnidirectional. The primary drawback of the rubber duck class of antennas is the ubiquitous presence of at least one set of nulls along the axis of the antenna in the E-Plane, shown to reach at least -25 dB in measurements.

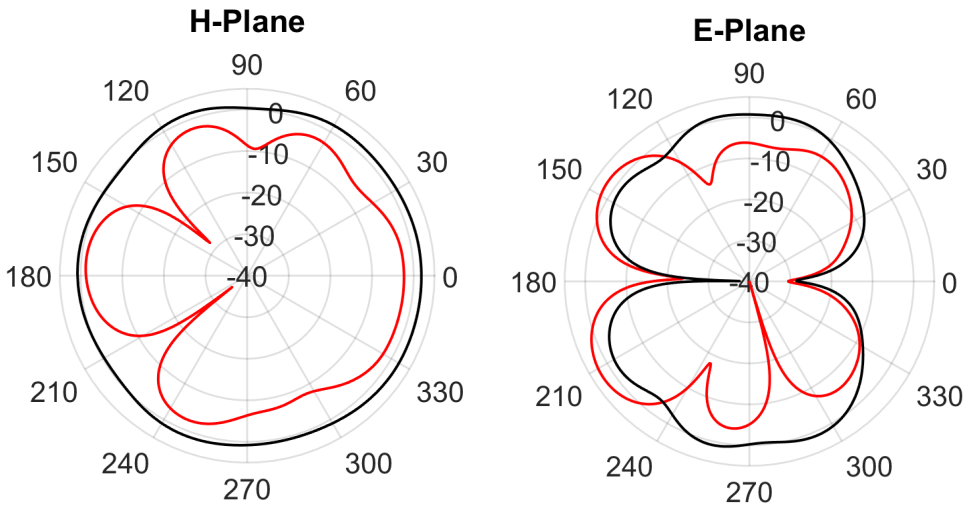

Figure 2.1: Measured radiation patterns for rubber duck antennas implemented with a half-wave dipole (black) and a coil loaded electrically small whip (red)

2.3 Cloverleaf Antennas

For non-conformal UAS applications, the cloverleaf antenna (also referred to as a skew planar wheel antenna in some forms) has been shown to provide a quasi-omnidirectional pattern [10]. The geometry of the antenna is comprised of three to five one-wavelength circumference wedge-shaped elements as depicted in Figure 2.2. The elements are spaced equally about the feed axis and are angled out of the base plane at an inclination of 45 degrees. These antennas are thus fairly large – occupying a cylindrical space with approximately a half-wavelength radius and quarter-wavelength height. The requirement of the elements to have a symmetric elevation from the base plane means that the antenna cannot be made conformal, but its simple construction and above average general performance makes it practically effective for SUAS applications. As a highly popularized antenna in the SUAS community with a single-plane quasi-isotropic pattern, it was briefly investigated to generate a baseline for comparison to the conformal antennas presented in this

work.

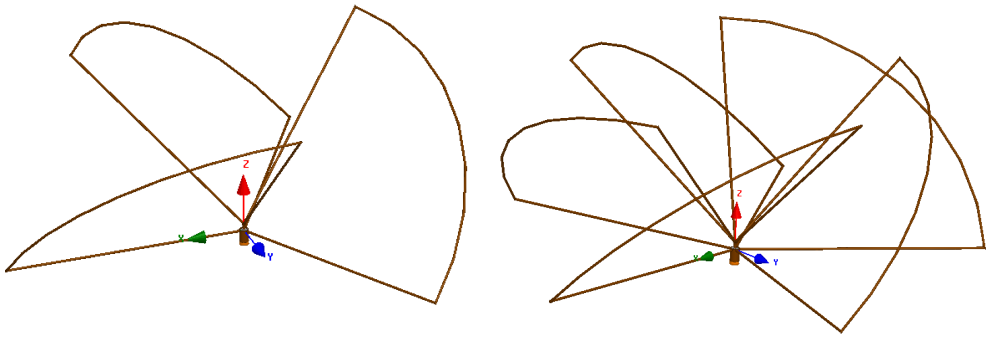

Figure 2.2: Cloverleaf antenna geometries: 3 element (left) and 5 element (right)

Simulations performed with HFSS show a radiation pattern comparable to that of a half-wave dipole with approximately 2.3 dBi gain, a minimum half-power beamwidth of 92 degrees, and circular polarization. The simulations also show an impedance match with a resonant input impedance of approximately 46.5 Ω and a 3 dB impedance bandwidth of at least 12%, increasing slightly with the number of elements. With three elements, there are substantial variations in the radiation pattern in the azimuth of as much as 1 dB. With five elements these variations are reduced to less than 0.2 dB in the azimuth and the overall pattern more closely resembles that of a half-wave dipole in both the azimuth and elevation planes. Figure 2.3 shows the simulated radiation pattern of the 3-element variation, the cut planes of which are overlaid with those of the 5-element variation in Figure 2.4. As with a dipole however, the cloverleaf antenna suffers from deep nulls in excess of -40 dB along its axis of symmetry. This renders the antenna minimally useful at range when trying to communicate either directly above or below the central axis of the antenna, with substantially degraded performance at any angle near the central axis as well. The skew planar antenna provides a large enough impedance bandwidth to cover the expected transmit and receive bandwidths with ease and nearly 100%

radiation efficiency in simulation. The cloverleaf antenna also offers circular polarization and a favorable consistency in azimuthal radiation. When form factor is negligible the cloverleaf antenna is nominally better than a half-wave dipole, but it is inherently non-conformal and impractical at frequencies below 1GHz for SUAS.

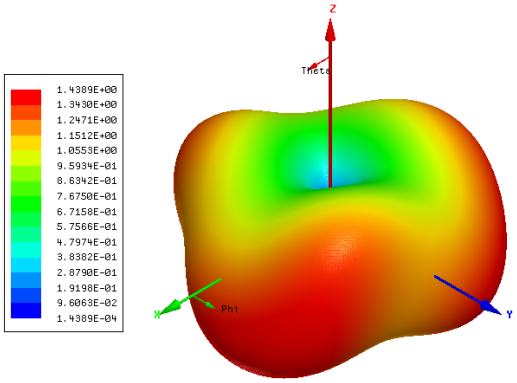

Figure 2.3: Far-field realized gain of the 3-element cloverleaf antenna

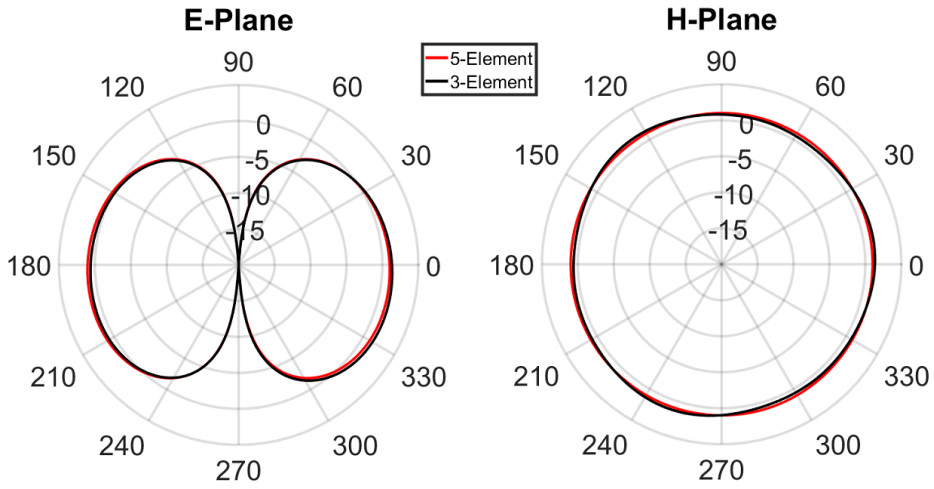

Figure 2.4: Far-field realized gain of 3-element and 5-element cloverleaf antennas emphasizing similarity to a dipole and slightly higher consistency of the 5-element antenna in the H-plane

2.4 Brief Survey of Conformal and Quasi-Isotropic Antennas

The development of isotropic radiators has been an area of open investigation for a number of years. For airborne communication systems, quasi-isotropic radiators are particularly useful in maintaining both air-to-air and air-to-ground links through a single communications chain. Conformal antennas have more recently become an open area of investigation, but their applicability to airborne communications is equally profound. When used in place of protruding or internal antennas, they may improve aerodynamics and allow for miniaturization of internal communications systems. Previous work has investigated a number of implementations of each of these characteristics and, although much less commonly, both simultaneously. This brief survey of previous work documents these characteristics.

An often implemented strategy for generating a quasi isotropic radiation is the distribution of current onto a radiating element that spans multiple orientations, each contributing in the direction of another element's radiation minima. In this way the sum pattern has minima much higher than that of any single element. This principle can effectively seen in the wrapping of a linear wire antenna structure in a plane [13] or about a 3-dimensional structure [14], [15]. By distributing the currents in three dimensions, as in Figure 2.5, the sum patterns of such an antenna achieve quasi-isotropy with with normalized minima at potentially greater than -3 dB. This method of distributed currents will be implemented and discussed in Chapter 4. A similar methodology exists for multiple connected radiators, typically of the same structure, that have orthogonal orientations to produce a pattern that has a net improvement on its quasi-isotropy [16].

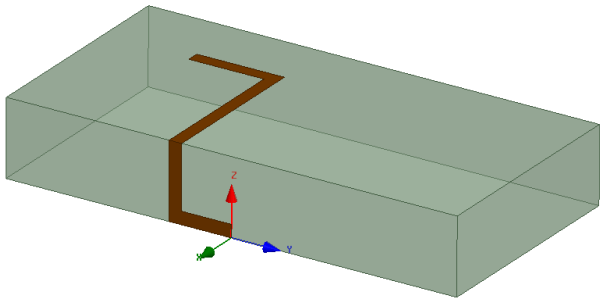

Figure 2.5: Example of perpendicularly bent monopole structure used to distribute currents strategically for generation of a quasi-isotropic pattern

The variety of antennas that are purely planar can attain conformal flexibility by fabrication on thin substrates. It has been previously shown that printed planar antennas on thin substrates can retain their insertion loss performance well up to a moderate degree of curvature when fabricated as such [17]. For the SUAS and frequencies under consideration in this work, the necessary degree of curvature for conformal antennas should remain in the bounds of this acceptable range. Arrays can produce levels of quasi-isotropy uncommon to singular radiators and, with added reconfigurability of elements, can attain uniquely adaptable patterns to fit system needs [18]. However, the form factors and highly variable structures between SUAS rule out many array styles as general solutions for at least some of the sub-1 GHz frequencies.

2.5 Summary

The most ubiquitous structure for SUAS applications is the rubber duck antenna. While it comes in many forms, the low end frequencies tend to dictate coiled whip implementations for size reduction. These structures tend to attain reduced effiencies with their size reduction and suffer the conventional nulls along their pri-

mary axis attributed to monopole designs. Cloverleaf antennas have slightly higher beamwidths, ideally perfect efficiency, and implement circular polarization. However, they suffer both from similar central radiation nulls and additionally require comparably large volumes of space to implement. Neither offer the quasi-isotropic pattern desired for this work.

A variety of structures have been developed to implement a quasi-isotropic radiation pattern. With the size constrained form factors presented by SUAS, arrayed structures are largely impractical and the desire for conformal applications rules out most 3-D implementations. Nevertheless, the technique of current distribution in three dimensions [14], [15] is of the utmost interest as it can be implemented at least partially in a planar configuration [16]. Aside from curving the antenna and substrate alone in free space, further considerations will need to be made for the variety of potential structures in the vicinity of a conformed antenna once it is on board an SUAS.

Chapter 3

Adapted Historical Omnidirectional Antennas

3.1 Introduction

In pursuit of conformal quasi-isotropic radiators, adaptations of well-established antenna structures for SUAS-constrained applications are first considered. As none of the antennas discussed as conventional for SUAS application were conformal, the implementation and effects of conforming of antennas to an example SUAS is explored with these established antenna structures. Impedance modified loop antennas are first pursed as a conformal alternative to half wave dipoles and the variety of rubber duck antennas previously discussed with a similar nominal radiation pattern. Modified crossed dipole structures are then explored as a means to achieve quasi-isotrpoic radiation while retaining the conformal structure desired. Methods for size-reduction are briefly for both antenna structures are investigated as a means to distance the designs from the outer limits of form factor presented by SUAS. Each antenna is examined for practicality and potential improvements to further improve their viability as SUAS antenna structures are discussed.

3.2 Impedance Modified Loop Antennas

3.2.1 Introduction

The first improvement on conventional SUAS antennas structures pursued was adding the trait of conformality. It is desired to at least maintain a comparable performance to a half wave dipole in the design. With design flexibility at a premium in accounting for the various challenges in conformally mounting antennas, particularly with the form factors SUAS constrain antenna designs to, impedance modifiable loop antennas were the first candidate investigated. Previous work has shown that the addition of a metal regions within the body or within close proximity of the exterior a loop antenna can drastically alter its impedance characteristics [19]. This methodology is shown to produce a impedance match at both a 50 Ω impedance with a variety of bandwidths based on the methodology used. Higher impedances, up to the nominal impedance of the loop, can be implemented and matched with N:1 chip baluns at the feed point. Metallization of the interior is first explored as it produces the minimal footprint given a nominal loop antenna. Alternative methods for impedance modification of the loops are then investigated to provide robustness when conformed and further expanded bandwidth to assess the merits of the internally impedance modified structures for their given size.

3.2.2 Design and Theory

The initial impedance modified loop antenna implements a rectangular patch equidistant on all sides from the main radiating element to produce an impedance reduction relative to their spacing, d_1 [19]. Optimization in HFSS suggested the widest bandwidths were achieved for the impedance modified structure when the width of the

radiator was approximately half its length and was thus restricted to this relationship throughout the investigated variations. The main radiating element is a full wavelength in circumference, resulting in the $\lambda/6$ by $\lambda/3$ footprint shown in Figure 3.1. This footprint approaches the practical limits of size for conformal applications on SUAS at 915 MHz for radio telemetry, but is highly applicable for the 2.4 GHz communications band. The gap parameter was kept at the size of the output pin gap, that of the SMA connector or chip balun, such that a minimal transition region was needed from the feed structure to the radiating element.

Simulations in HFSS were performed on a structure with $t = 1.5$ mm, $gap = 1.5$ mm, and $d_2 = 2$ mm. The simulations indicated that the input impedance of the modified loop structure at its resonance is approximately a linear function of the % of the area inside the loop that is filled by the metal patch. This relationship, depicted in Figure 3.2, has a correlation coefficient of at least 0.995 over the values tested. The most linear region is for any percentage of fill greater than 50 %. This region corresponds to simulated resonant input impedances at or below 125 Ω. Thus the investigation of impedance modified loops were targeted at 50 Ω and 100 Ω variations.

It was desired to model the impedance modified loops numerically to aid in rapid prototyping and allow for development of antennas without full wave simulation. Linear regression was performed on the simulated range greater than 50% fill, noted as being the most linear, to begin this process. In the range of fill %age between 50 and 95 %, the simulated input resistance is linearly modeled as approximately

$$R_{in} = 271.32(1 - F) - 1.46; \tag{3.1}$$

This impedance should correlate to a full wave rectangular loop which with an

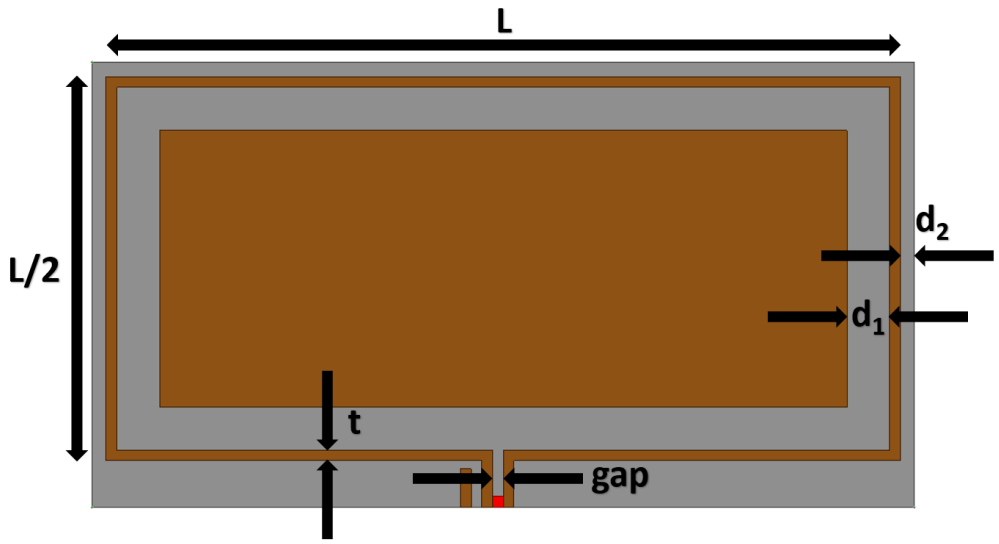

Figure 3.1: Geometry and design parameters of the nominal impedance modified loop antenna

impedance of approximately 260 Ω when having no metal fill and 0 Ω of impedance when the space is almost completely filled and loaded to an effective short circuit. If the function is linear over the entire range of fill %age, the impedance would reasonably span from zero to the nominal resonant loop impedance, R_0. Thus the calculated linear model from the linear regression was adjusted to these values and rearranged in terms of the fill %age. The corresponding decimal fill %age necessary to generate a specific impedance is thus

$$F = 1 - \frac{R_{in}}{R_0}; \tag{3.2}$$

Some inaccuracy is expected in the lower extent of fill values where the simulation shows linearity does not necessarily hold. Using the area of the interior space and the area of an arbitrary patch, the distance needed between the patch and radiator can be determined by solving functions of the geometry. Note that the relationship is inherently simplified here by the given 2:1 side length ratio. The spacing d_1 from

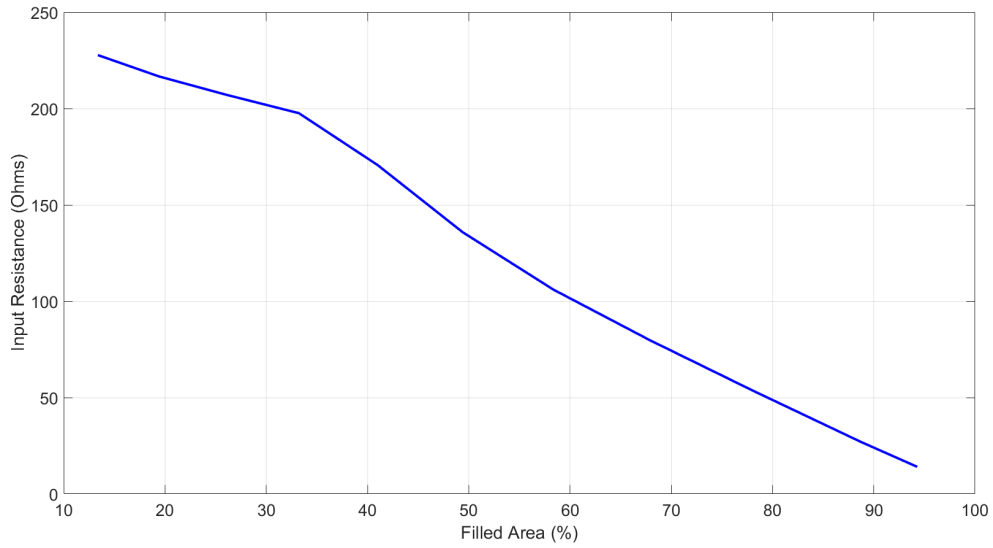

Figure 3.2: Input resistance trends for varying % fill of the patch in the impedance modified loop at the corresponding resonance for each respective value of d_1

the ground plane needed to realize this fill %age with the given geometry is

$$d_1 = \frac{1}{8}(3L - \sqrt{16F(L-t)(L/2-t) + L^2} - 4t); \tag{3.3}$$

For $t << \lambda/6$, the length of the short side of the radiator in this example, the closed form approximation for the uniform fill to element spacing given a desired impedance R_{in} is then

$$d_1 = \frac{1}{8}\left(\lambda - \frac{\lambda}{3}\sqrt{8\left(1 - \frac{R_{in}}{R_0}\right) + 1}\right); \tag{3.4}$$

Using Equation 3.4 to design an impedance modified loop at 50 Ω and 100 Ω resulted in fill to radiator spacings to 3.67 mm and 7.73 mm, respectively. Both variations were simulated in HFSS with the constant parameters noted above and the resulting resonant impedances were 46.65 Ω and 104.67 Ω. Using the exact form for d_1 in Equation 3.3 provided spacings of 3.58 mm and 7.55 mm, resulting

in impedances of 48.98 Ω and 100.79 Ω, respectively. This implies the thickness of the lines have a non-negligible effect on the estimated impedance of the structure as it changes the effective area, but it may still be closely approximated so long as the thickness is a small fraction the size of the lesser radiator dimension. The unsimplified form of the equation, however, shows excellent convergence with simulation with a maximum deviation of nearly just 1 Ω. For full-wave loops that do not have a 2:1 rectangular dimension ratio, the predictive equation may be used in an unsimplified form. It estimates the fill to distance ratio as

$$d_1 = \frac{1}{8}\left(\lambda - \sqrt{-16(F-1)L^2 + 8(F-1)L\lambda + 8Ft(2t-\lambda) + \lambda^2} - 4t\right); \quad (3.5)$$

and the same method of approximation for a trace thickness much smaller than the shortest rectangular dimension yields a distance of

$$d_1 = \frac{1}{8}\left(\lambda - \sqrt{16\frac{R_{in}}{R_0}L^2 - 8\frac{R_{in}}{R_0}L\lambda + \lambda^2}\right); \quad (3.6)$$

The applicability of this relationship to rectangular loops with rectangular ratios other than 2:1 was briefly investigated. A square variation with a 1:1 side ratio as well as an elongated variation with a 3:1 side ratio were tested. The same nominal parameters of $t = 1.5$ mm, $gap = 1.5$ mm, and $d_2 = 2$ mm we maintained. The square loop had a simulated resonant impedance of 130.29 Ω. When simulated with the full and approximated values of d_1 from Equations 3.5 and 3.6 and a desired impedance of 50 Ω, impedances of 56.41 Ω and 57.47 Ω were observed, respectively. For the elongated loop with a 3:1 dimension ratio, a nominal impedance of 317.74 Ω was observed in simulation. Impedances of 54.55 Ω and 54.86 Ω were recorded for the full and approximated values for d_1. These two variations show

that the equations may also be fair predictors for other geometries, but the maximal deviation of up to 15% from the intended impedance implies that further refinement may be needed in the numerical model to generally extend it as such. This degree of error would suggest that the quality of impedance match and bandwidth of the antenna may be substantially reduced. With such a large nominal bandwidth, however, compared to the 3% fractional bandwith maximum observed on the crafts in our test fleet, this method of design should still be fully applicable with power losses from impedance magnitude mismatch. Alternatively, one might stick with the nominal 2:1 size ratio which has excellent agreement with the model and is specifically characterized in this work.

3.2.3 Measurements and Integration of Chip Baluns

The rectangular loop antenna that was loaded down to operate at an input impedance of 50 Ω showed consistency with the simulation in return loss magnitude despite a realized operating frequency approximately 10 MHz above the simulated design. Both operated with approximately 7% bandwidth and had a 40 dB return loss at the peak impedance match. The loop antenna designed for 100 Ω experienced a near equivalent frequency upshift but was not as consistent in return loss characteristic with the simulation. The measured peak impedance match was approximately 7 dB less than in simulation and thus the 3 dB bandwidth realized was 11% as opposed to the simulated result of 14%. Based on follow-up testing of 1:1 transformer chip baluns on the 50 Ω loops, this was determined to be caused in part by the additional small inductance across the coils of the transformer not explicitly designed for in simulation.

The measured radiation patterns of the 50 Ω rectangular loaded loop are shown

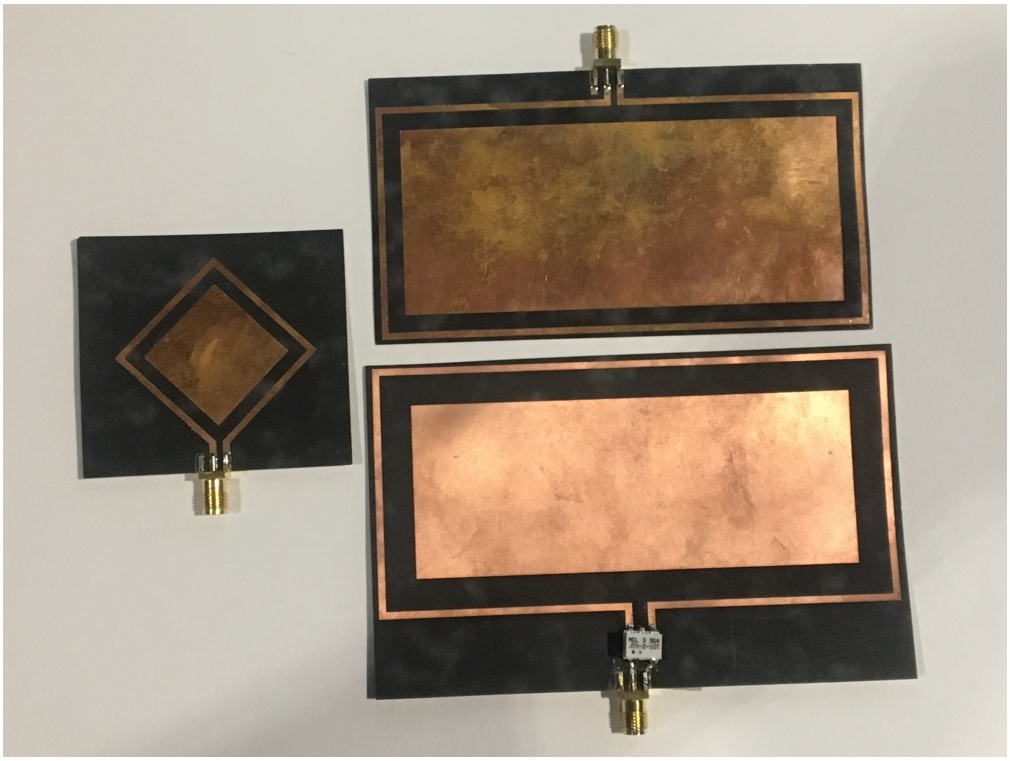

Figure 3.3: Fabricated Loop antennas: 2.4 GHz 50 Ω diamond loop (left), 915 MHz 50 Ω rectangular loop (top), and 915 MHz 100 Ω rectangular loop with 2:1 chip balun (bottom)

in Figure 3.5 to match with simulation well in shape but with a slight reduction in all-around realized gain. This slight reduction in gain is in part attributed to the lossy low inductance chip balun used to transform the feed from coax to balanced twin lead. The antenna is quasi-isotropic in the elevation plane with a maximum variation in the radiation pattern of 1.96 dB. The half-power beamwidth in the azimuthal plane is, however, fairly narrow at 76 degrees. The loop radiation pattern is thus comparable to a dipole with slightly higher half-power beamwidth, but is advantageous due to its much wider impedance bandwidth over a typical rubber duck antenna and its ability to conform to a surface.

When a 1:1 balun with 18 μH of inductance was implemented in the feed structure of the antenna, a marked frequency shift of the optimal operating frequency

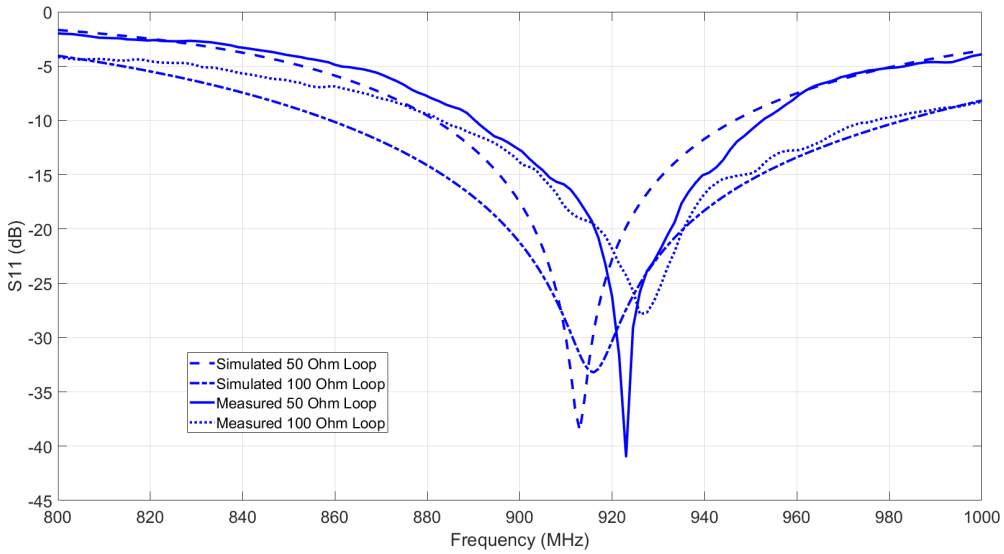

Figure 3.4: Simulated and measured results for the fabricated rectangular loops

was observed in measurements. This frequency shift is theorized to be a result of changing the effective port impedance by adding an inductive load at the source. Thus the antenna exhibits a resonance where it is both matched most closely to 50 Ω with an opposite reactance. The operating frequency of a 50 Ω variation of impedance modified loop was reduced down to approximately 745 MHz from the design frequency of 915 MHz. This result is in stark contrast with the results attained from both the directly fed 50 Ω variation and 2:1 balun fed 100 Ω variations previously discussed, each having higher realized operating frequencies compared to simulation. Additionally, the measured impedance bandwidth is greater than that of the higher frequency simulated and measured variations. Practically, when considerations are made for approximately 2 dB of insertion loss given as typical of the high inductance chip balun, the fractional bandwidth is maintained throughout the frequency shift. Direct scaling down of the antenna was performed to counteract the realized frequency shift which provides a method for downsizing an otherwise electrically large antenna.

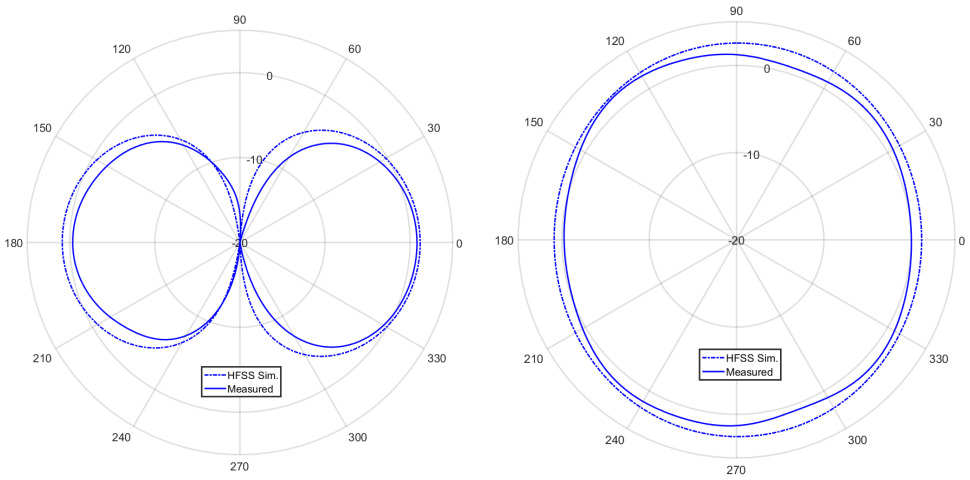

Figure 3.5: Measured versus simulated Azimuth (left) and Elevation (right) radiation patterns for rectangular 50 Ω loop

3.2.4 Investigation of Optimal Placement

The impedance modified loop antennas discussed herein were simulated in HFSS backed by air, Rogers 5880 dielectric, and comparable plastics to those used for the airframe of the test platform, the 3DR IRIS. The IRIS has a substantial number of electronics and otherwise conductive components throughout the craft as well as a sizable battery pack in the underbelly of the craft. As these components fall in or very near the near field of these antennas, the impact of conformal placement on the craft for the radiation patterns and insertion loss of the antenna was investigated. Full wave simulation of the entire of the structure was impractical so the antenna was tested in situ positioned as centrally as possible on the top and bottom as well as wrapped conformally about the upper rear half the rear of the craft for comparison. The semi-rear position of the craft was selected because, despite being near the GPS transmitter, is otherwise the most distanced location from conductive bodies or other interferers throughout the entirety of the craft surface.

The impedance modified loops did not display a substantial relative improve-

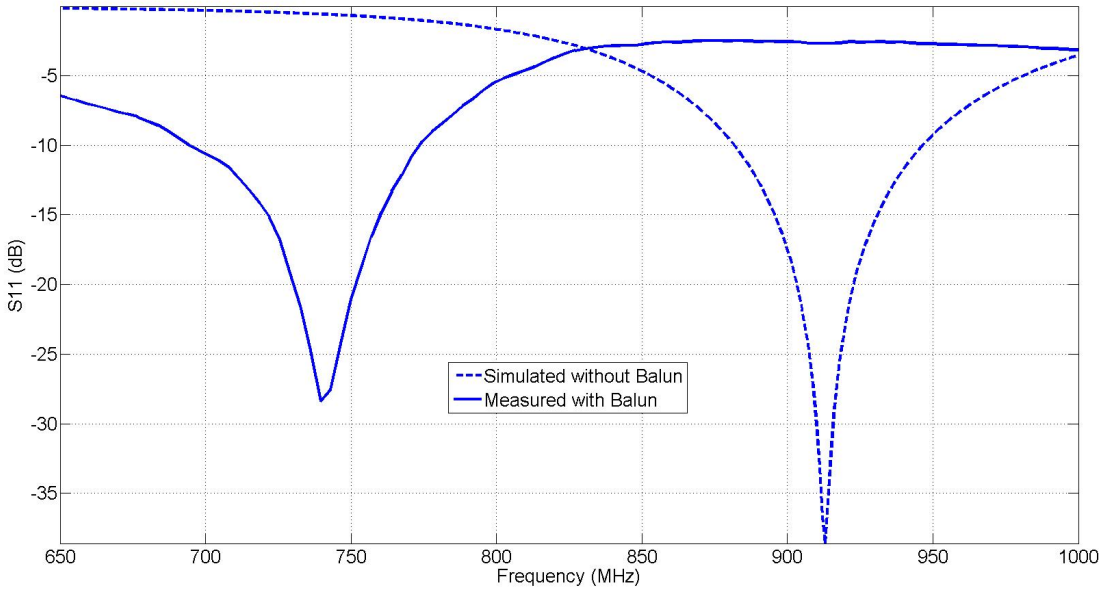

Figure 3.6: Simulated rectangular loop with a lumped port excitation and measured rectangular loop with a 1:1 high inductance (18 μH) chip balun

ment between the positions for the overall radiated power in any of the three positions in the E or H planes. The performance in the H-Plane of the antenna in particular was fairly consistent regardless of position with a maximal variation of approximately 4 dBi, as shown in Figure 3.8. In the E-Plane, the rear position exhibited both the least significant null and the most quasi-isotropic pattern, closely followed by those of the bottom placement. The rear thus was the slightly more favorable antenna position for achieving the goals of this work when working with loop antennas.

For considering the optimal placement in terms of insertion loss, the primary metrics are the frequency shift from loading effects and the ability of the antenna to maintain maximal performance at and in a band around the center frequency of the nominal design. The measurements depicted in Figure 3.9 show the insertion loss for an impedance modified loop designed for a higher frequency expecting a

minor downshift in frequency from conformal loading despite placement. Placing the antenna on the bottom under the battery, as in Figure 3.7, is shown to both substantially shift the frequency and affect the frequency response. While the top side placement of the antenna has a comparable frequency trend for the insertion loss, the frequency shift for the rear placed antenna is less than half that of the top side placement. Thus with both the most favorable overall radiation pattern and insertion loss trend, the rear placement is considered to be optimal of those tested. This assessment agrees with initial theorized choice of inclusion of rear placement.

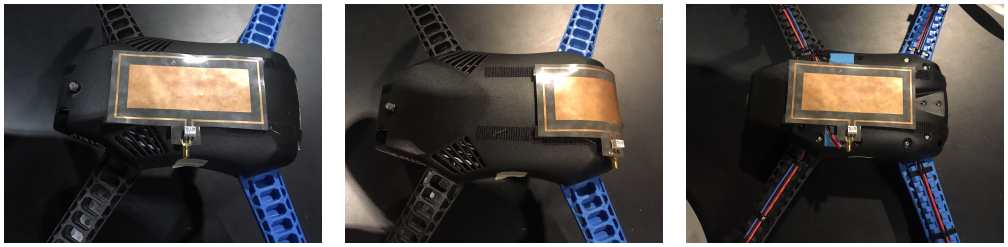

Figure 3.7: Conformally mounted impedance modified loop antenna in the top (left), rear (middle), and bottom (right) positions as mentioned

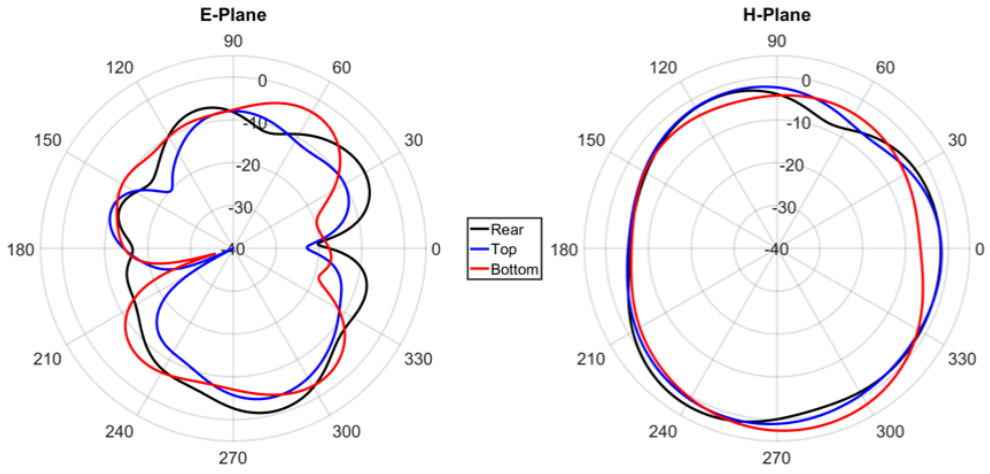

Figure 3.8: Radiation pattern E-Planes (left) and H-Planes (right) of 100 Ω loop with 2:1 balun conformally attached to IRIS aircraft in top, bottom, and rear locations showing impact of placement on antenna functionality

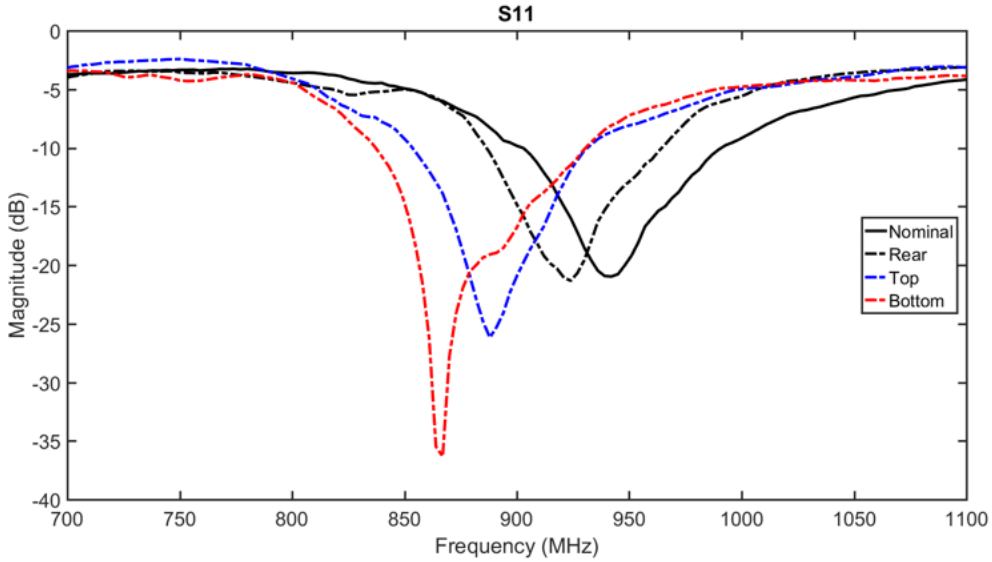

Figure 3.9: Insertion loss of 100 Ω loop with 2:1 balun conformally attached to IRIS aircraft in top, bottom, and rear locations showing impact of placement on antenna functionality

3.2.5 Alternative Loading Schemes

As it was established that the loading effects on the impedance modified loop antennas were significant enough to substantially shift the frequency and alter the performance of the antenna, an investigation was performed to determine whether these effects could be used in place of the metallic load originally implemented. This would account in advance for loading effects and ensure the antenna operates close to nominal designs if implemented successfully. Figure 3.10 shows the simulation setup of the antenna placed over the plastic shell containing the battery and two FR4 boards. For this simulation it was theorized that the battery would be the primary loading object on the antenna due to its size and proximity. The figure also shows the simulated insertion loss of the antenna, which is neither as wideband nor as well matched as that of the 100 Ω variation with a 2:1 balun but should remain fairly consistent when it is placed conformally in a manner close to that of the

simulation. The simulated radiation pattern is shown to become more directive in this configuration in Figure 3.11, attaining a peak to minima difference of approximately 10 dBi in the H-Plane. While this would wholly not achieve the desired quasi-isotropic trait desired, it provides a method by which loop antennas might be implemented for basic air to ground communications in siutations where internal structures substantially hinder conformal performance of the basic impedance modified loops and still maintains viable amounts of aerial radiation for air-to-air communication.

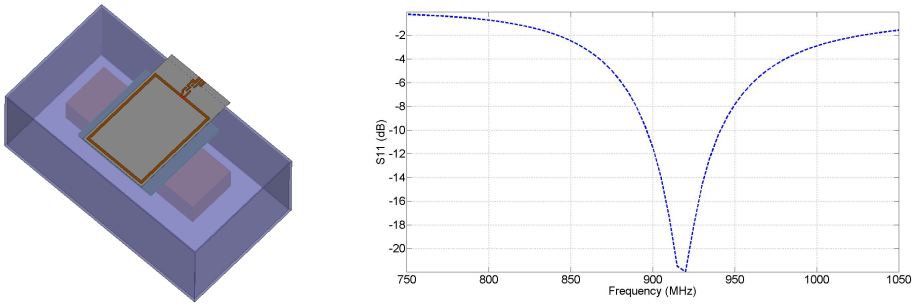

Figure 3.10: Battery and dielectric loaded loop antenna geometry (left) and simulation results (right)

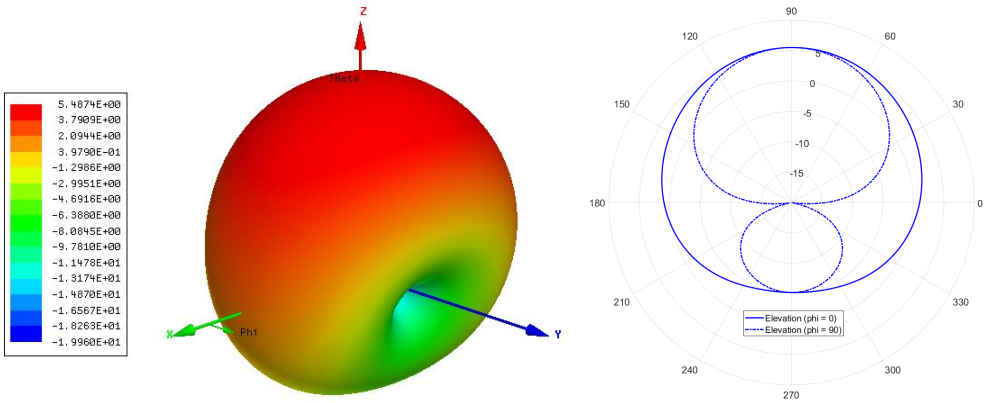

Figure 3.11: Full radiation pattern (left) and perpendicular elevation plane patterns (right) for simulated battery and dielectric loaded loop antenna in dBi

The craft internals loaded loop antenna was fabricated and measured confor-

mally on the IRIS aircraft with a low inductance chip balun at the feed point. The IRIS has a rounded airframe at the edges, so it is expected to have a slightly altered insertion loss response. Figure 3.12 shows that, for its intended position on the bottom of the craft, the antenna had a vastly different insertion loss pattern than simulated or expected. Subsequent removal of the battery had a comparably minimal effect on the insertion loss relative to the simulated effect of its addition, with a realized change of no more than 1.5 dB over the entire band measured. This indicates that the circuit board and electronics between the antenna and battery had a much more substantial contribution to the loading in contrast to how they were simulated. An alternate test was performed with the antenna positioned on the top of the craft where a conglomeration of electronics rest at approximately the same distance as the battery in the simulation. This top-side test is shown in Figure 3.12 to produce an insertion loss pattern tat resembles that of the simulation, albeit at a frequency approximately 80 MHz lower. This indicates that, while the theory of loading the antenna with craft internals may be a viable solution, a more complex model of the variety of components in the vicinity of the antenna is needed to properly approximate the loading effects in simulation.

3.3 Modified Crossed Dipole Antennas

3.3.1 Introduction

A conceptually simple antenna structure that has been well-documented in the literature to improve upon the radiation isotropy of a standalone half-wave dipole and provide circular polarized radiation is the crossed dipole [20]. Both previous work [20], and simulations that were completed in HFSS in the present work show that by aligning two dipole-like radiators perpendicularly and feeding them in quadrature,

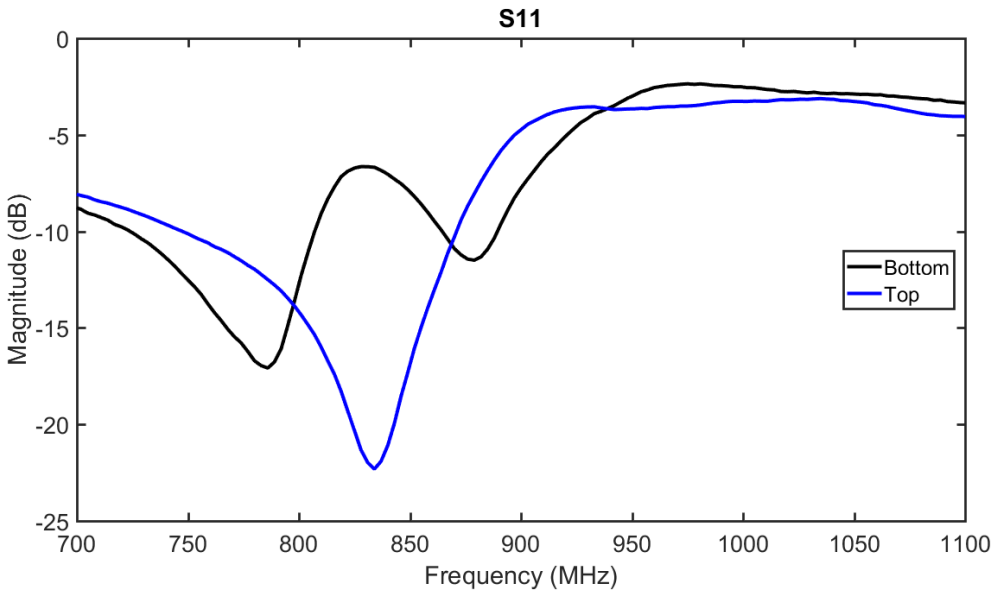

Figure 3.12: Measured insertion loss of the craft internals loaded impedance modified loop antenna in its intended position on the bottom of the craft and an alternate position on the top center of the craft

a quasi-isotropic radiation pattern with maxima at broadside of the antenna plane is produced. As with the half-wave dipoles in the rubber duck class of antennas, if small and conformal qualities are desired in an antenna, a linear set of dipoles will be comparable in size to the entire fuselage of some SUAS below 1 GHz, making them nominally impractical for these applications. Thus, size-reduction techniques were pursued to reasonably implement a pair of crossed dipoles as an electrically-small conformal structure.

3.3.2 Design and Theory

The minimal surface area for a half-wave crossed dipole pair is approximately a 0.325 λ square. To reduce the electrical size of the antenna, each of the four elements of the crossed dipole is bent perpendicularly at halfway along its length. In doing so, capacitance is added to the structure and the resonant frequency is corre-

spondingly shifted upwards. The resulting frequency offset is corrected by scaling the size of the elements proportionally to the ratio of the realized frequency to the desired frequency of 915 MHz. When re-tuned, the antenna occupies a space of approximately a quarter-wavelength square. To further decrease the footprint of the antenna, inductive elements can be added at the end of each element to load the antenna down and elicit a frequency downshift. The inductive loads can be realized as helical wire elements or meander lines in practice depending on the desired fabrication method. The addition of the inductors allows for tunability at the cost of impedance match and bandwidth. Choosing 30 MHz (the maximum typical bandwidth of the IRIS aircraft used for testing) as a low end limit on bandwidth, joint optimization of inductor dimensions and antenna size was performed in HFSS to produce the smallest possible structure fulfilling the bandwidth constraint. The resulting antenna occupied a square area of just over 0.2 λ on a side. This provided a roughly 60% reduction in the overall form factor of the antenna. The geometry of each stage in the process is depicted in Figure 3.13 and the corresponding reflection coefficient trends are overlaid in Figure 3.14.

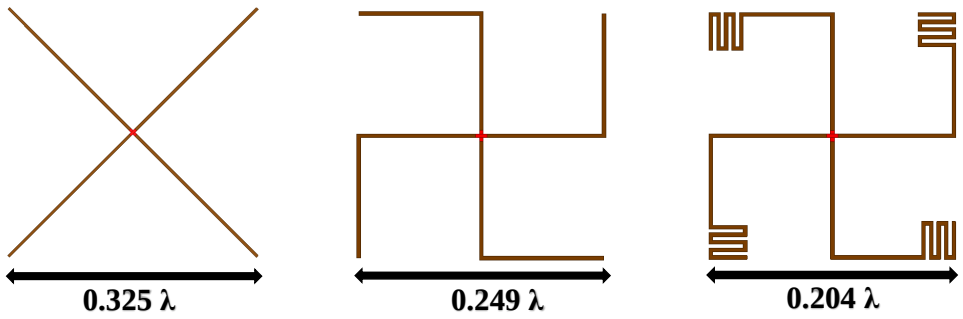

Figure 3.13: Progression of linear crossed dipoles into meander-line loaded crossed dipoles and corresponding electrical size of minimal square package at each stage

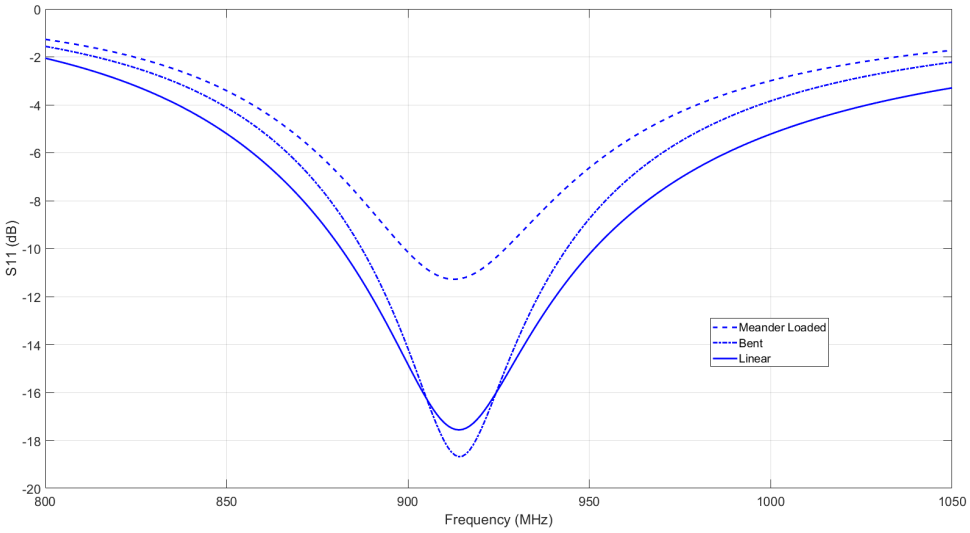

Figure 3.14: Reflection coefficient magnitude for the discussed stages of development for the modified crossed dipole antenna structure

The antenna parameters for the antenna were examined for the antenna both with two separate or a conjoined port, which support the intended circular polarized variation with a 90 degree phase offset between the elements of the crossed dipoles and a dual polarized variation fed from the center point for analyzing impedance, respectively. Figure 3.15 shows that the antenna does provide quasi-isotropic radiation in the phase offset case with a half power beamwidth of 140 degrees and a maximum normalized null depth of -3.36 dB, as noted in Table 3.1. Radiation patterns were simulated for both a meander-line and helixcal inductor-loaded variation were tested for investigation of fabrication practicality. Their performance is nearly identical with the helical inductor variation having approximately 0.25 dB more gain in the direction the helixes are coiled. The system impedance bandwidth when fed by a single port is approximately 20 Ω, which is much lower than desired for matching to the 50 Ω system standard on most SUAS. The element-wise impedance bandwidth when fed seperately is 3.2 %, or approximately 30 MHz at the investigation frequency of 915 MHz. The structure also maintains a very high

radiation efficiency of at least 97 % through each of the two intermediate and final geometries.

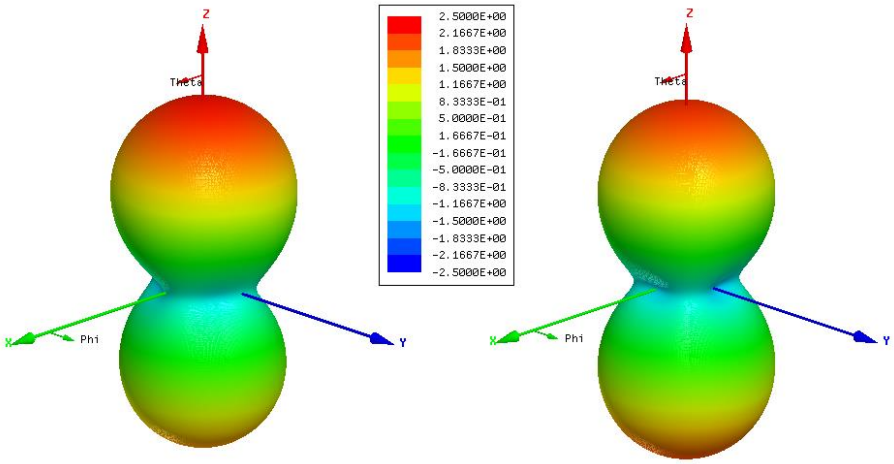

Figure 3.15: Simulated radiation pattern for the modified crossed dipoles implemented with helical wire inductor loads (left) and planar meander line inductor loads (right)

Table 3.1: Inductor-Loaded Cross Dipole Antenna Parameters

Half Power Beamwidth	Maximum Null Depth	Radiation Efficiency	Input Impedance	Impedance Bandwidth
140°	-3.36 dB	0.97	20.38 Ω	3.2%

While the performance of the inductor loaded crossed dipole antenna does initially appear to be favorable for conformal applications from its antenna metrics, the needs for practical implementation complicate it in system integration. The antenna impedance is designed such that a single element is well-matched to 50 Ω, thus the parallel system of crossed dipoles has an impedance of approximately 20 Ω. To match to a 50 Ω system, either the elements need to be designed for a much higher individual impedance or a transformer needs to be included in the feed structure. A 2:1 chip balun would be a possible dual-purpose solution, but would need to be designed around loading effects on the system impedance by putting an inductive

transformer element on the input of the structure. Investigation of specific methods for increasing the overall system impedance to 50 Ω are currently a topic of future work, but would further complicate the antenna structure regardless. Additionally, quadrature feeding requires integration of a phase shifting mechanism into the transmit and receive chains which adds a non-negligible layer of design complexity to the implementation.

3.4 Conclusions

In the consideration of historical omnidirectional antennas, it was shown that the structures investigated provided either the quasi-isotropy or implementation simplicity desired for SUAS applications, but failed to achieve them simultaneously. Impedance modified loop antennas provided a simple to implement design with a straightforward impedance design model. Modified crossed dipoles were harder to practically implement but demonstrated the first case of the desired quasi-isotropic radiation pattern.

Impedance modified loop antennas were shown to provide a bandwidth greater than that necessary for operation on our test craft and those with similar telemetry links. This offers a favorable degree of flexibility when conforming to a craft incites frequency and magnitude changes in the insertion loss. Measurements showed that, while the nominal loops are large at a full wavelength in circumference, they may be substantially reduced in area by the inclusion of a high inductance balun inciting a frequency downshift. This increases their applicability to size constrained SUAS applications. A novel impedance model was developed for the prediction of impedances based on the area filled by the loading patch and this model was extended to rectangular loops of arbitrary side ratios. This model shows excel-

lent convergence with the nominal 2:1 size ratio model, predicting the impedance within 2%. Extension of this model to arbitrary sizes increases the error to as much as 15%, suggesting refinement of the model may be necessary. Additionally, due to the impedance modification method, it was shown that the craft can theoretically be used as a load which may eliminate the majority of negative effects of conformal placement and rather use them advantageously. The loops did not however generate the quasi-isotropic pattern desired to enable unrestricted directional communication, which prompted further investigations into antennas that might accomplish that.

As a well-established antenna structure in literature and large-scale practice, crossed dipoles were known to provide a quasi-isotropic radiation pattern. However, size reduction was deemed necessary as half-wave radiators are the telemetry frequency were impractical. The use of symmetric quarter-wave bending and inductive end-loading were shown to reduce the form factor of the antenna by more than half and allow for an impedance match to 50 Ω for the two-port system. Each of the size reductions did however come at the cost of impedance bandwidth, settling in the final form at only 3%. The main flaw of these antennas was the implementation difficulty. The requirement of a phase shifting mechanism and some method of impedance transformation for implementation with a single feed over-complicated the otherwise simple structure and was counter to the goal of minimizing the overall footprint. The investigation of the dipole structures did however provide valuable insight into the outcome of conforming dipoles to structures and aided in the development of the following antenna.

Chapter 4

Curved Folded Dipole Antenna

4.1 Introduction

Pursuit of a more quasi-isotropic pattern led to investigation of a curved folded dipole antenna (CFDA). This structure was first investigated as an electrically-small substitute to a typical dipole by Scheldorf in a form with considerable end capacitance due to the inclusion of metallic plates [11]. More generally, investigations of curving a folded dipole structure in its azimuthal plane [21][11], conforming modified folded dipole structures to dielectrics [17], and characterization of strip folded dipoles with a feed line [22] have been previously performed. These investigations did not, however, seek the generation of a quasi-isotropic radiator from such structures as is desired here. The antenna geometry presented here is approximately that of a folded dipole antenna circularly curved in its own plane as two half elements with a short gap and a linear connection for a feed line added.

This structure is shown to exhibit a 3 dB beamwidth consisting of at most the entire far field when quasi-isotropy is prioritized, while still maintaining a 50 Ω impedance match over at least 20 MHz. The bandwidth is shown to be adjustable up to at least 80 MHz at the cost of some of the quasi-isotropy. It is also shown to be physically flexible about its axis of symmetry up to an angle of curvature of

45° with minimal effect on its performance. The great deal of design flexibility and high degree of quasi-isotropy make it an ideal candidate for SUAS applications.

4.2 Design and Theory

The CFDA is defined by five parameters depicted in Figure 4.1: the two trace widths, the spacing of the traces, the spacing at the feed point, and the angle of curvature in the plane. The impedance is varied by changing the angle of in-plane curvature, defined as the angle formed by the mean path length arc from the edge of the linear extension for the port to the corresponding gap edge of the antenna. The impedance varies from approximately 275 Ω to a range of 40 Ω to 55 Ω from the linear folded dipole configuration to the fully circularized configuration shown in the figure. Table 4.1 details the nonlinear relationship between the angle of curvature and the input impedance or radiation efficiency. Small deviations in curvature angle from a linear folded dipole incite minimal changes while equal variations near full semi-circular curvature force much more pronounced impedance and radiation efficiency variation. There is also a notable variation in the operating frequency for a 50 Ω port, as depicted in Figure 4.2 . The operating frequency point shifts upwards until a curvature angle of approximately 150° and then recedes to approximately that of the linear folded dipole at 180°. At 180° of curvature, the largest dimension of the antenna is approximately 0.17 λ. A reduction in the maximal dimension by a factor of approximately 3 is thus achieved over a linear folded dipole at the cost of generally encompassing more surface area.

As the antenna is formed into the semi-circular configuration, the distributed current is wrapped symmetrically about the axis of curvature. Given that any small section of current on a linear folded dipole contributes a biconcave disk of radia-

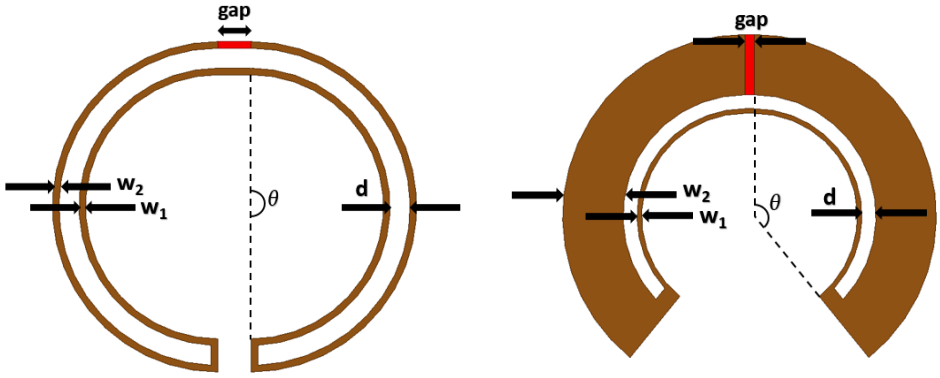

Figure 4.1: Geometry and design parameters for the curved folded dipole antenna in the nominal equal width configuration (left) and a wideband configuration (right)

Table 4.1: Peak Real Impedance and Radiation Efficiency Trends for In-Plane Curvature in Air and on 10mil Rogers 5880 Substrate at resonant frequency

Curvature Angle (deg)	Peak Real Impedance (Ω)		Radiation Efficiency	
	Air	Rogers 5880	Air	Rogers 5880
1.000	275.77	252.99	0.986	0.980
45.000	254.11	230.75	0.985	0.978
90.000	188.54	166.47	0.978	0.972
120.000	135.35	118.64	0.970	0.961
150.000	85.58	75.06	0.951	0.937
180.000	47.93	43.14	0.908	0.881

tion to the net pattern, the equivalent result for the CFDA is doing so in about a semi-circle effectively filling in part of the radiation null that results from the currents correlated with the direction of the feed. As with a linear folded dipole the current distribution on the CFDA is approximately that of a half-cosine centered at the feed. Thus full isotropy still cannot be achieved even at 180° of curvature. The close proximity of the arm ends adds a slight end capacity which aids in achieving a slightly more evenly distributed current pattern [11]. For the CFDA, the E and H planes depicted in Figure 4.3 are defined as though the radiator was a linear dipole likewise fed across the gap. The progressive lessening of the nulls in the E-Plane through added curvature is depicted in Figure 4.4. By the same principle, compo-

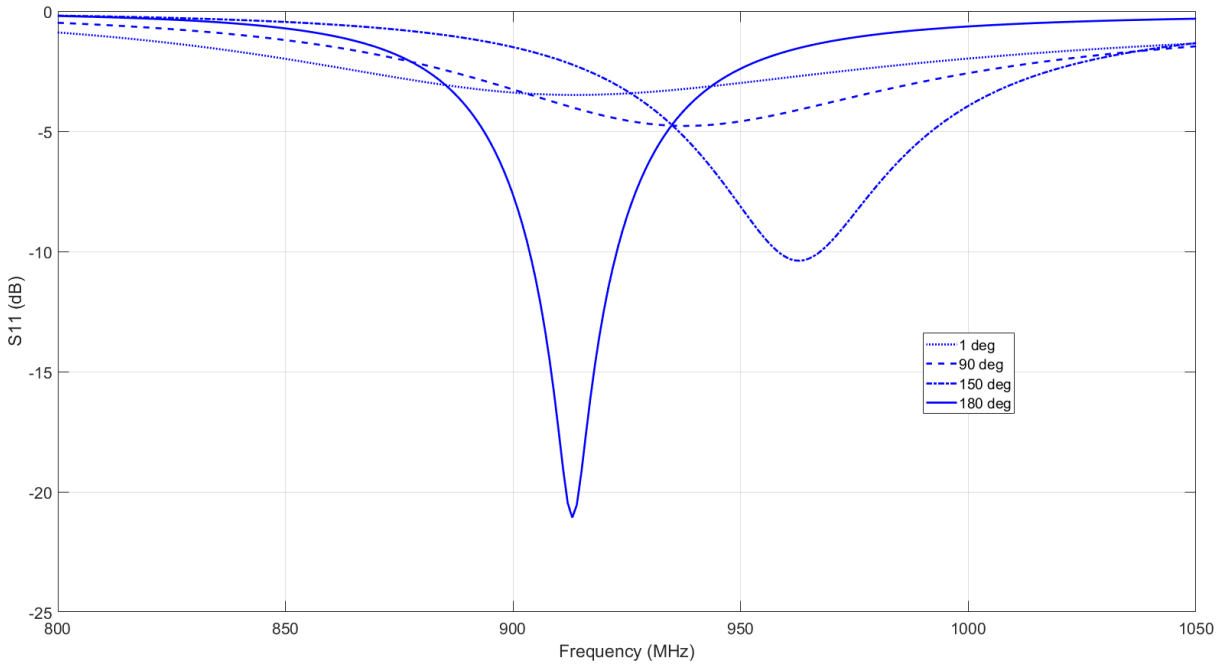

Figure 4.2: Reflection coefficient for selected angles of curvature for a 915 MHz design with a 50 Ω feed port in HFSS

nents of the current direction now exist perpendicular to those generated at the feed point for any point along the curved wire so the H-Plane radiation pattern trends towards an oblong shape rather than a circle for an increasing degree of curvature. For the nominal equal line width configuration in Figure 4.1, the normalized E-Plane radiation minima will remain lower than that of the H-Plane, but simulations in HFSS have indicated that excess curvature past $\theta = 180°$ and manipulation of unequal lines may lead to the E-Plane minima potentially overtaking that of the H-Plane. Further work is needed to assess if the point where they become equal could be considered the optimal radiation pattern that most closely approximates isotropy.

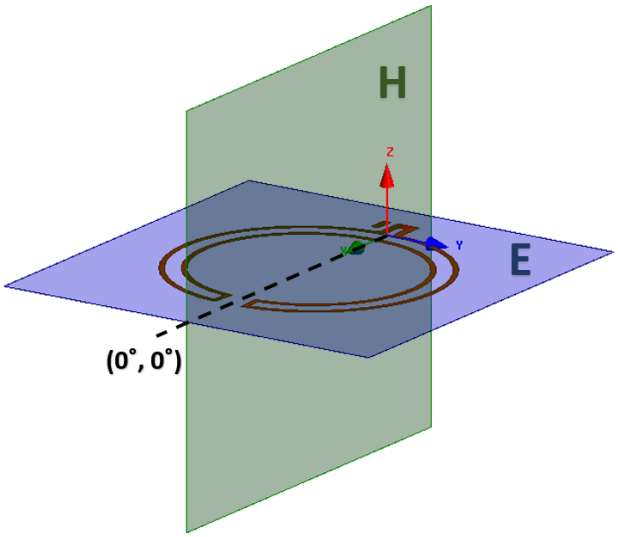

Figure 4.3: Depiction of the E-Plane and H-Plane for far field radiation for the CFDA with both planes referenced in angle to the symmetry line of the radiator geometry

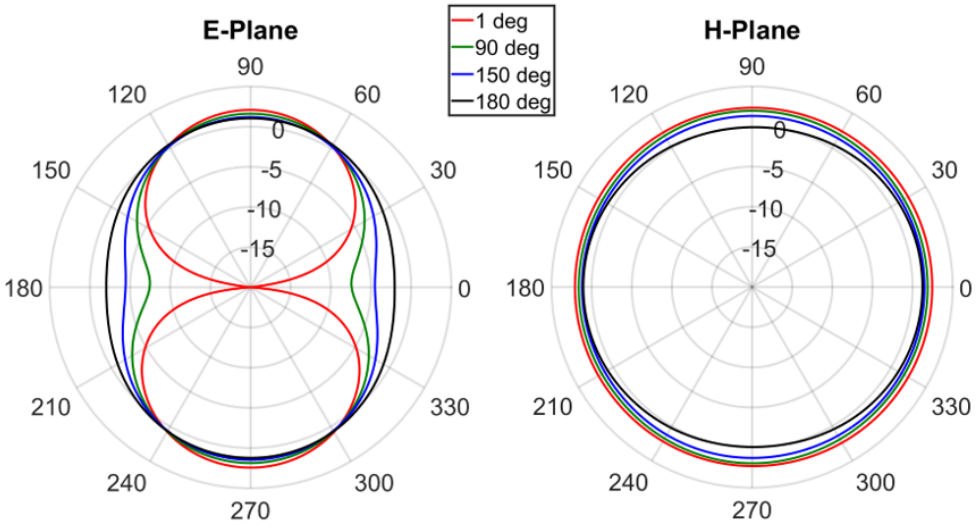

Figure 4.4: Progression of radiation pattern with increasing angle of curvature in the E-Plane (left) and in the H-Plane of the unconformed antenna (right)

Using the assumption that the curved radiator consists of a series of small dipole elements directed tangentially to the portion of the antenna to which they corre-

spond, an approximate pattern can be generated for predicting the behavior at a given angle of curvature. Each small element has a contribution to the pattern scaled by the current at that point on the CFDA. Simulations in HFSS show that the antenna exhibits quite nearly the current distribution of a linear folded dipole's first mode with the surface currents at the ends of the antenna having a magnitude less than 1% of those at the feed point. Assuming the linear portion of the antenna at the feed approaches 0, the realized gain for a given angle in the E-Plane for the model, M_θ, based on the E-Plane pattern of an ideal dipole, I_θ, for N divisions of the radiator is

$$M_\theta = \sum_{k=0}^{N-1} I_{\theta - k\frac{\pi}{N}} |cos(\frac{\pi}{N})| \frac{1}{N}; \tag{4.1}$$

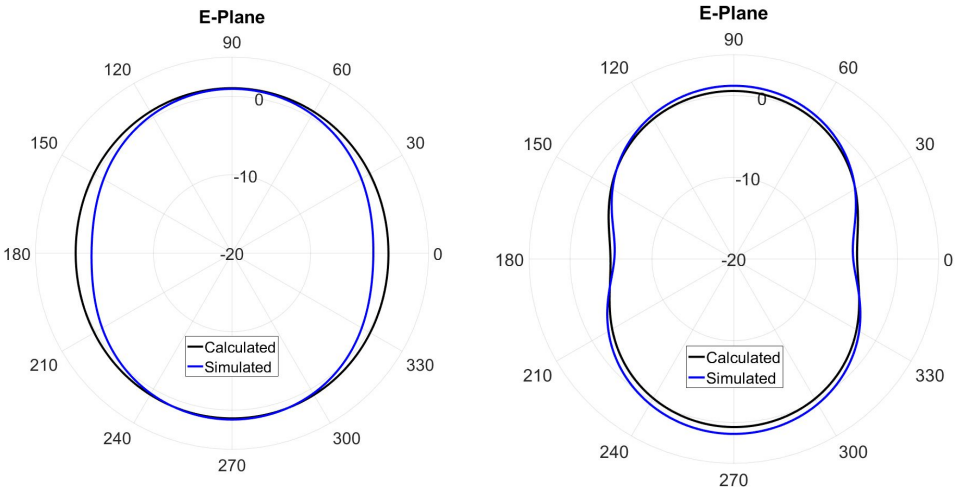

Figure 4.5: E-Plane radiation pattern comparison for the segmented currents numerical model and simulation with 180 degree (left) and 135 degree (right) angles of curvature

An investigation of conformally bending the antenna in free space was performed to characterize the fundamental effects on the antenna of conforming to the shape of various airframes. Based on the crafts in the test fleet (IRIS, IRIS+, Bix3) and expected antenna positioning on said crafts, the conformation was modeled as

though the intended surface was cylindrical. The conformal angle, depicted in Figure 4.6, is defined herein as the conformation to a cylinder of a radius such that half of the antenna covers an arc angle equal to the conformal angle. In other words, it is the arc angle covered by half the antenna when it is uniformly curved about its axis of symmetry. The CFDA was tested from a planar configuration to a half cylindrical form at a ϕ of 90°.

As with bending the original folded dipole in its own plane to form the curved planar structure, the radiation efficiency and real impedance values are shown in Table 4.2 to trend downward with increasing conformal angle about the air cylinder. A notable degradation in a match to 50 Ω consequently reduces the impedance bandwidth when the conformation becomes more significant. The antenna also experiences a moderate shift in the resonant frequency as the antenna is conformed all the way to the half-cylinder configuration. These effects show a similar nonlinear relationship to conformal angle as that seen in curving the folded dipole in-plane where the same increase in curvature angle has much more pronounced effects as it reaches the maximum considered. The variations apparent in Table 4.2 and Figure 4.7 show that this is is favorable for the given implementation because so long as the antenna is not conformed beyond 45°, it maintains a very similar performance to the planar configuration with an acceptable degree of frequency shifting. The acceptable degree of frequency shifting for the SUAS involved in this investigation is roughly 5 MHz at a center frequency in the 915MHz band shown in Figure 4.7, as that is the excess bandwidth the nominal CFDA exhibits over the 3DR IRIS minimal transmit bandwidth of 10MHz. For the platforms discussed, the antenna is small enough relative to the package that conformation should not need to exceed this threshold regardless of position. Thus, the performance can be approximated as that of the antenna placed flat upon the material surface.

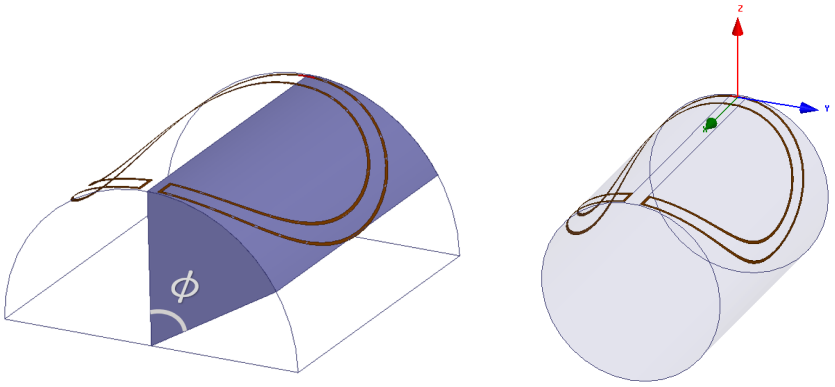

Figure 4.6: Depiction of the conformal angle at ϕ = 60° (left) and the half-cylindrical bending geometry with a conformal angle ϕ = 90° (right)

Table 4.2: Impedance and Radiation Efficiency Trends with Conformation

Conformal Angle (deg)	Real Input Impedance (Ω)	Radiation Efficiency
1.000	41.91	0.897
20.000	41.21	0.892
45.000	40.38	0.881
70.000	33.98	0.858
80.000	30.99	0.845
90.000	28.04	0.829

4.3 Antenna Performance Flexibility

Linear folded dipole antennas can be impedance modified by adjusting the wire spacing or wire widths. The corresponding impedance scaling factor [23] relative to a half wave dipole for a given folded dipole geometry with center to center wire spacing of S is

$$K = \left(1 + \frac{log(2 * S/w_2)}{log(2 * S/w_1)}\right)^2; \tag{4.2}$$

It was experimentally discovered that adjusting size ratio of w_2 to w_1 for a CFDA could have a substantial effect on its bandwidth. Since the geometry of the CFDA includes wires of different length, the applicability of the folded dipole impedance

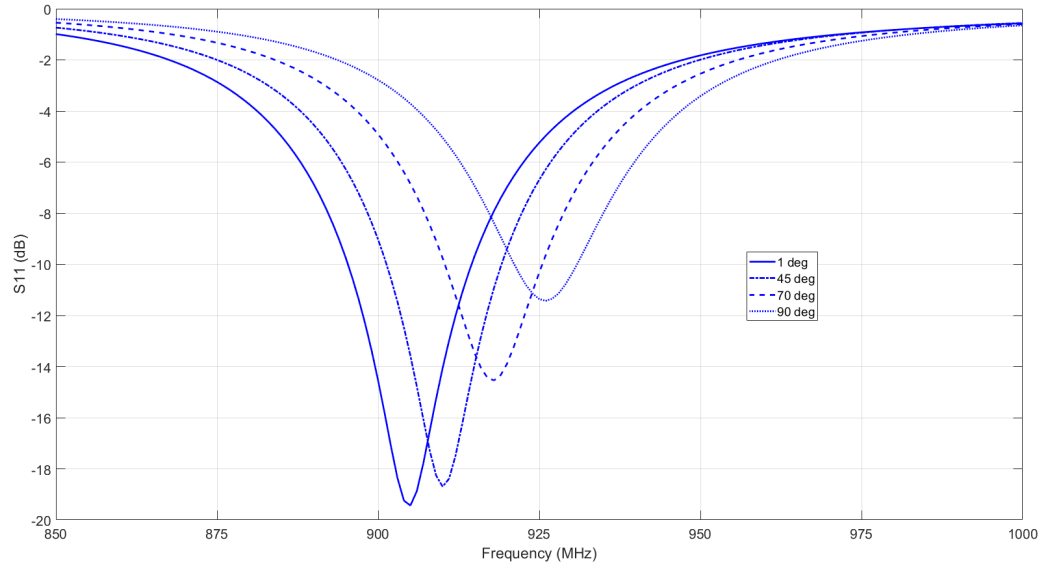

Figure 4.7: Reflection coefficient for discrete conformation angles for a 915MHz design

scaling in projecting the impedance change from adjusting w_2 was merited. When the wire widths are the same, the nominal scaling factor is exactly 4. Since the CFDA is intentionally tuned to 50 Ω to begin with, the scaling equation must be scaled down by a factor of 4 to be implemented to reference the desired 50 Ω characteristic impedance. For a CFDA with a real input impedance of R_0 in an equal wire width configuration, the real input impedance of a corresponding unequal width configuration would thus be

$$Re(Z11) = R_0 \left(1 + \frac{log\left(2 * \frac{w_1/2+d+w_2/2}{w_2}\right)}{log\left(2 * \frac{w_1/2+d+w_2/2}{w_1}\right)}\right)^2; \tag{4.3}$$

Simulations were performed in HFSS for a range of w_2 from 1 mm to 15 mm with constant geometry otherwise of $w1$ =1mm, d =3mm, and $\theta = 176°$. The simulations show excellent convergence with the modified impedance scaling formula, as depicted in Figure 4.8, despite the substantial divergence from the typical folded dipole geometry. The average and maximum disparities in real input impedance for

the range simulated were 1.39 Ω and 2.71 Ω, respectively. With an accurate predic-

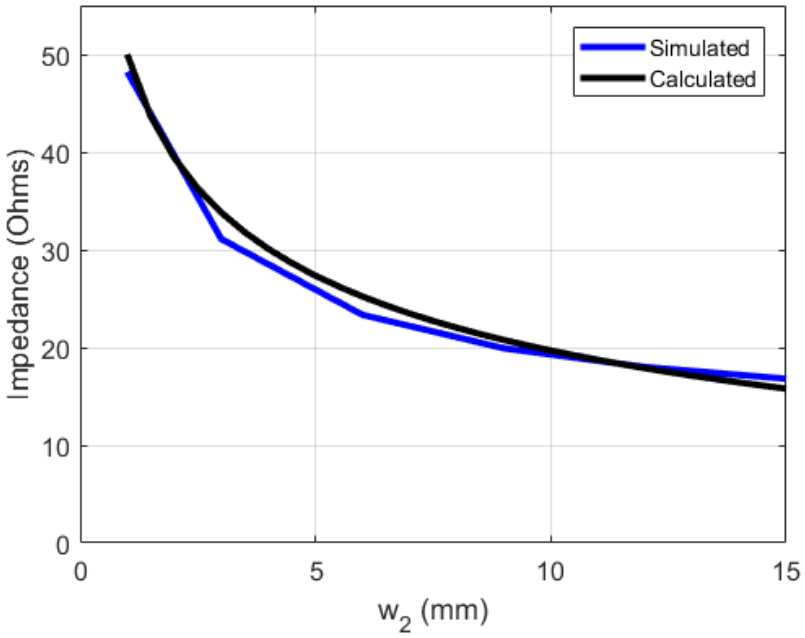

Figure 4.8: Comparison of CFDA impedance variations projected by conventional folded dipole impedance scaling to simulations, resulting from adjusting w_2 with d =3mm, w_1 =1mm, and $\theta = 176°$

tor for the impedance with unequal wires and established trends for the impedance for a given angle of curvature θ, the CFDA can be optimized for bandwidth by implementing offsetting impedance changes to retain a 50 Ω match. The enlarging of w_2 provides for a more gradual frequency response for the reactance while retaining a comparable real input impedance at and around the resonance, diverging only at the upper end of the frequency band. The impedance frequency response of the nominal 20 MHz design and designs with up to four times the bandwidth are depicted in Figure 4.9 with a notable variation in the slopes of the dashed reactance curves apparent. The performance trade-off of implementing this technique is the recession of the antenna radiation pattern towards that of a linear folded dipole as the angle of curvature is reduced. The nominal 20 MHz antenna design has a

minimum realized gain of approximately -2.2 dBi in the E-Plane and Figure 4.10 shows that the corresponding minima reaches -5.4 dBi with the 80 MHz variation, the geometries of which are shown in Figure 4.1. The H-Plane has less substantial maximal variations at approximately 1.7 dBi as the pattern transitions from oblong to circular and finally oblong in the perpendicular direction, that of the symmetry plane. Table 4.3 additionally shows that the antenna continually grows in physical size with increasing bandwidth through the use of this method. The size of the lines increases much faster than the height of the antenna decreases due to reducing the angle of curvature such that the wideband 80 MHz variation requires twice the rectangular area to encompass it compared to the nominal 20 MHz variation. Both the constriction of the radiation pattern and the increased form factor are substantial costs to consider for SUAS applications that would ideally dictate fitting on a small craft and radiating uniformly.

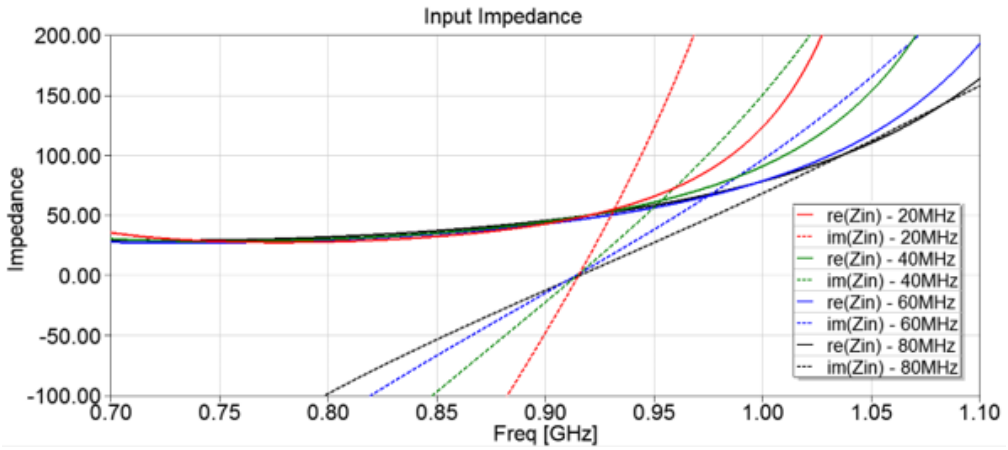

Figure 4.9: Impedance progression of the CFDA as w_2 is increased and θ is decreased to create offsetting impedance changes and achieve increased bandwidth

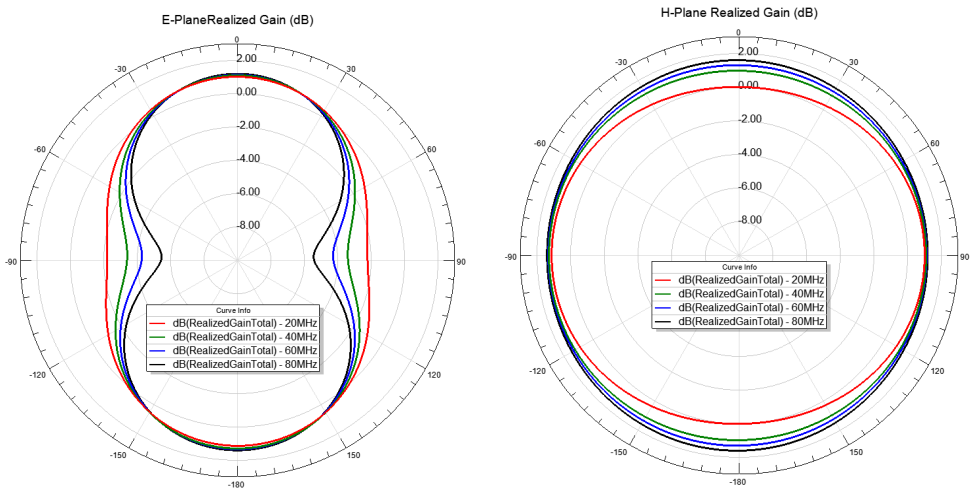

Figure 4.10: Radiation pattern progression of the CFDA as w_2 is increased and θ is decreased to incur offsetting impedance changes and achieve increased bandwidth

Table 4.3: Size of CFDA variations resulting from increasing bandwidth through varying the line widths and decreasing the angle of curvature to compensate for impedance changes

Antenna	Rectangular Dimensions	Rectangular Surface Area
20 MHz	52 x 55 mm	28.6 cm^2
40 MHz	61 x 66 mm	40.2 cm^2
60 MHz	65 x 75mm	48.8 cm^2
80 MHz	69 x 84 mm	58.0 cm^2

4.4 Measurements

The nominal CFDA and wideband variation with 20 MHz and 80MHz of bandwidth, respectively, were both fabricated on 10 mil Rogers 5880 dielectric and measured for insertion loss and radiation characteristics. Figure 4.11 shows the nominal variation of the CFDA as well as prototype wideband and 2.4 GHz band implementations. The insertion loss characteristics of two 915 MHz band CFDAs attached to bazooka baluns are shown in 4.12. The nominal variation shows a high degree of convergence with the simulated insertion loss characteristic, varying by a maximum of 2 dB at the peak impedance match with a 2 MHz up-shift from simulation. Away from the operating frequency, the simulation and measured results are within 1 dB when accounting for the slight frequency shift. While the wideband variation shows a similar convergence of no more than 2 dB of disparity in the upper portion of the frequency band, the measured and simulated results diverge by as much as 4 dB off the operating frequency, when considering the frequency shift. The frequency shift for the wideband variation is 8 MHz, the same % of the bandwidth as the nominal variation, but occurs with an 11 dB disparity in peak impedance match. The measured wideband variation does still achieve a minimal insertion loss 10 dB lower than that of the nominal variation at -30 dB and -20 dB, respectively.

Measurements of the radiation patterns of the two variations of the CFDA were performed with 915 MHz bazooka baluns. The anechoic chamber measurements were calibrated using a wire dipole tuned to 915 MHz on the same length bazooka balun. In the E-plane, the nominal CFDA design showed excellent convergence in Figure 4.13 for the 90 to 270 degree half plane, but diverged as much as 2.5 dBi on the opposite half-plane. The H-plane was even more consistent, varying by no

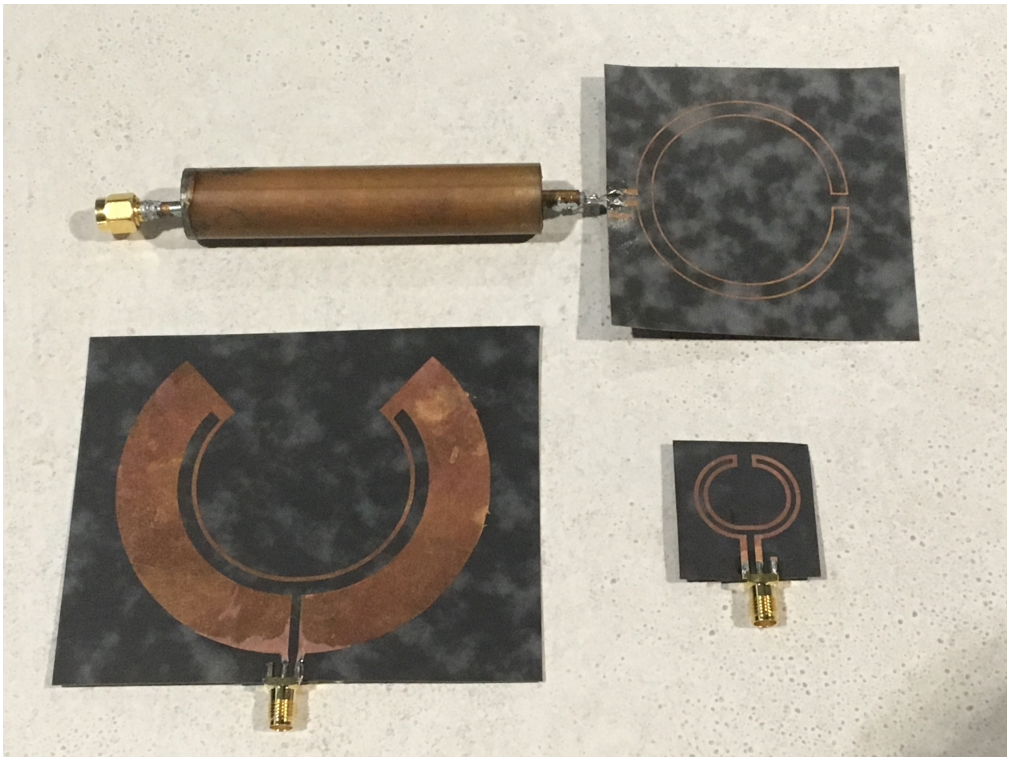

Figure 4.11: Fabricated 915 MHz nominal CFDA with bazooka balun (top), 915 MHz wideband CFDA (left), and example 2.4 GHz CFDA (right)

more than 1.2 dBi about its entirety. The nominal CFDA design exhibited a maximal realized gain of 1.8 dBi. The wideband CFDA showed a similar excellent adherence to the expected pattern in the H plane depicted in Figure 4.14, not exhibiting a disparity of higher than 1 dBi. The E-plane, however, was more volatile in the divergent half plane and consistently wavered up and down in gain relative to simulation with a maximum disparity of 1.5 dBi above or below the simulation. The wideband CFDA exhibited a maximum gain of 2.5 dBi. As predicted by the investigation of wide-banding the CFDA, the wideband variation had a more constricted E-plane and more fully circular H-plane as the geometry recedes slightly towards that of a linear folded dipole.

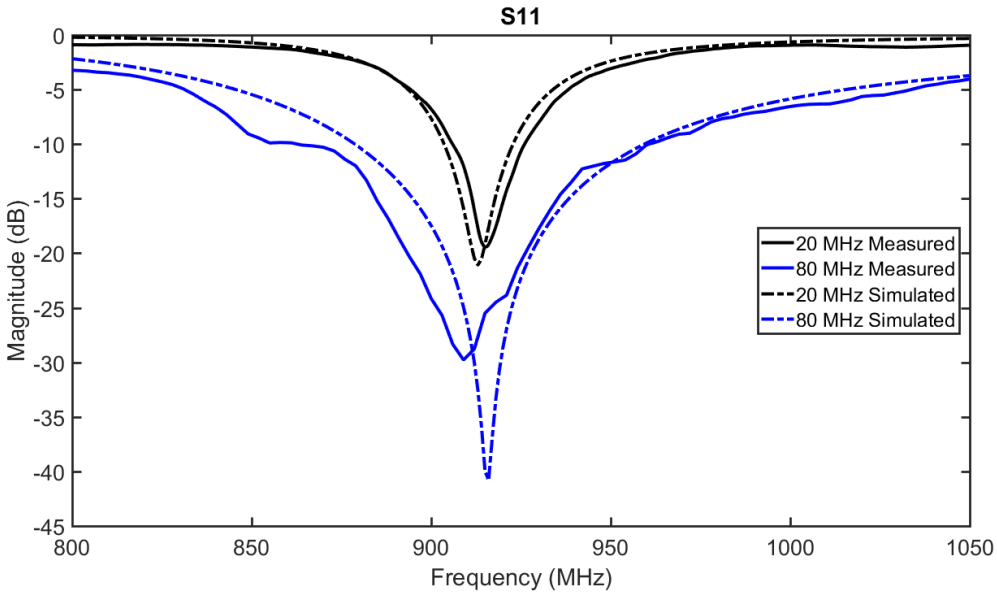

Figure 4.12: Simulated and measured results for the fabricated nominal and wide-band CFDA variations

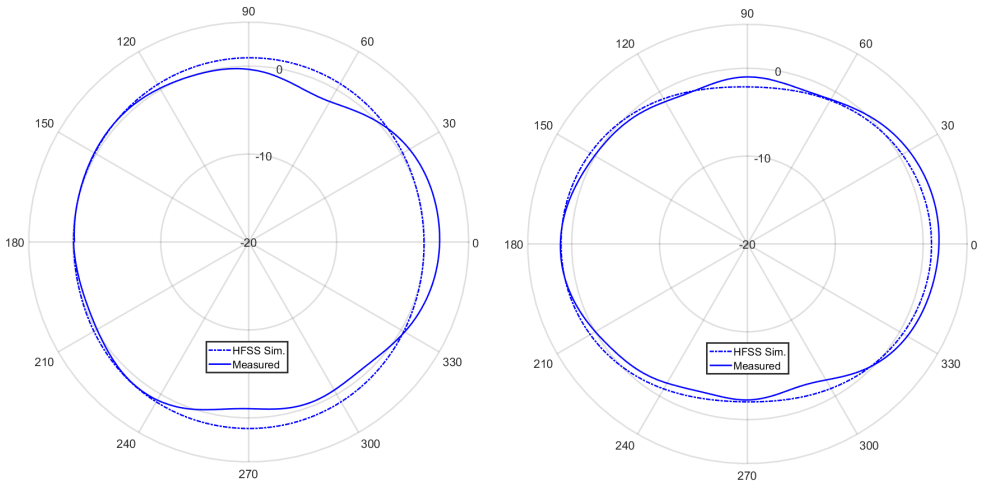

Figure 4.13: Measured versus simulated H-Plane (left) and E-Plane (right) radiation patterns for thin nominal quasi-isotropic CFDA

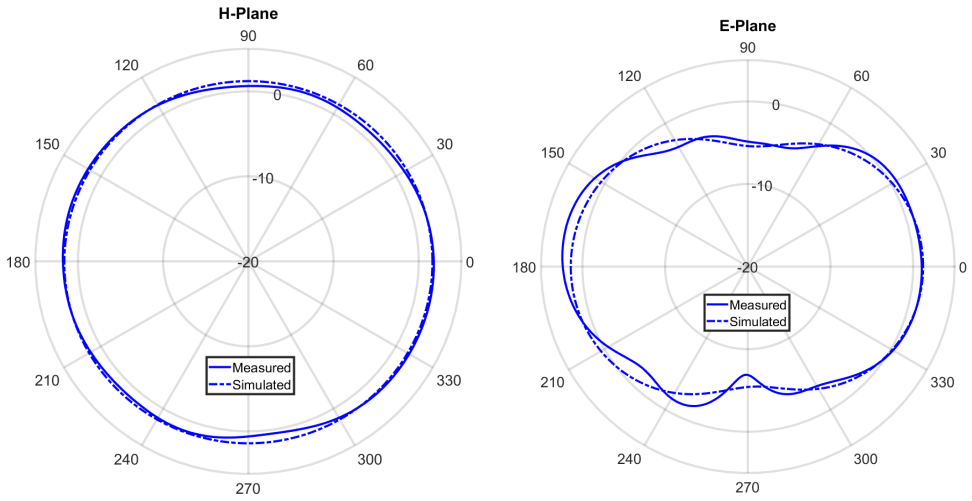

Figure 4.14: Measured versus simulated H-Plane (left) and E-Plane (right) radiation patterns for wideband variation of the CFDA

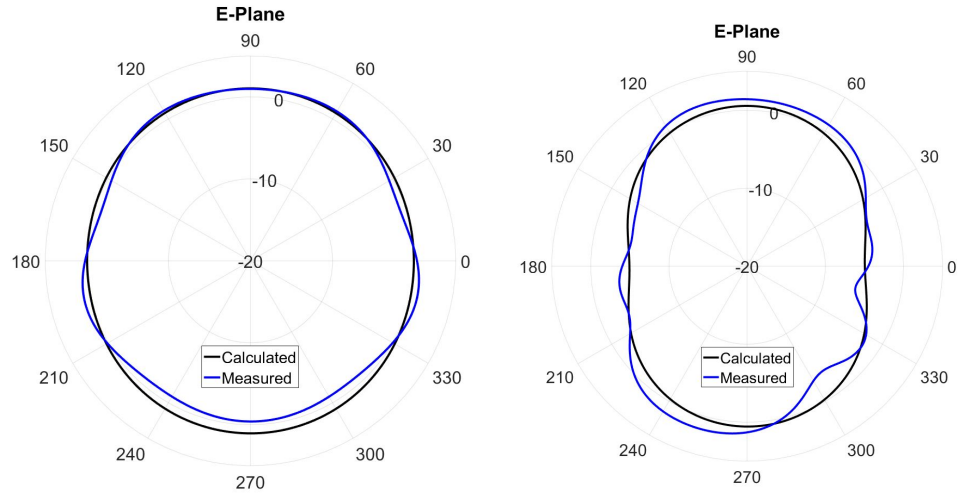

Figure 4.15: E-Plane radiation pattern comparison for the segmented currents numerical model and measurements of the nominal CFDA design (left) and the wideband design (right)

4.5 Investigation of Optimal Placement

As with the impedance modified loop antennas discussed herein, the CFDA variations were simulated in HFSS backed by air, Rogers 5880 dielectric, and compara-

ble plastics to those used for the airframe of the non-idea IRIS test platform. Full-wave simulation of conformally placed CFDA variations were likewise impractical, so the same positions were used to test the extremes of internal craft loading of the antenna. Initial simulations and measurements suggested great variation of influence on the narrowband and wideband variations, so results were taken separately.

The CFDAs were judged on average realized gain and quality of quasi-isotropy for the E and H planes. For the nominal narrowband CFDA, there was a marked difference between the realized gains of the top and bottom placements compared to the rear placement. In both the E and H planes the local maxima for the rear located measurements were as much as 10 dBi higher than those of the top or bottom placements, as depicted in Figure 4.17. The H-Plane of the rear variation in particular exhibited the highest realized gain of all variations tested throughout the entire plane, although the E-Plane performance exhibited this behavior for over three-quarters of the plane. The rear placement was thus determined to have the best radiation characteristics for conformal quasi isotropic applications.

The CFDA variations are electrically small so the magnitude of insertion loss across the frequency band was the primary comparison metric for measurements of S11. The secondary metric was the magnitude of the frequency shift compared to the bandwidth. The magnitude of the insertion loss over the associated frequency bands were comparable from the nominal to rear and top positions, with the minima raising 4 dB and bandwidth increasing 15 % for the latter, as shown in Figure 4.18. The bottom placed measurements show significant degradation of the insertion loss such that no point in frequency reaches below -8 dB. As the other two positions have comparable performance in their bands, the rear measurements exhibit approximately half the frequency shift from nominal and is thus designated the best performing variation for insertion loss. As it thus has the preferred performance in

both radiation pattern and insertion loss, it was designated the optimal placement of those tested.

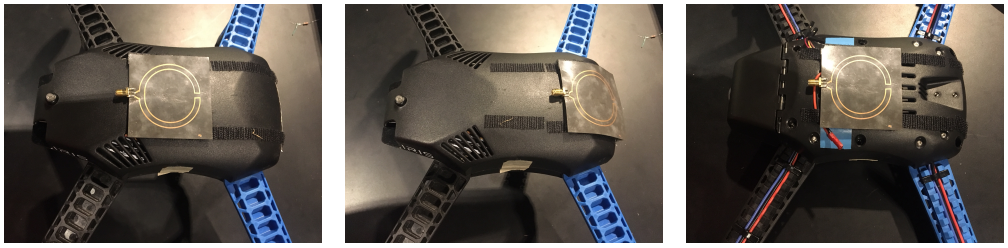

Figure 4.16: Conformally mounted 20MHz bandwidth CFDA variation in the top (left), rear (middle), and bottom (right) positions as mentioned

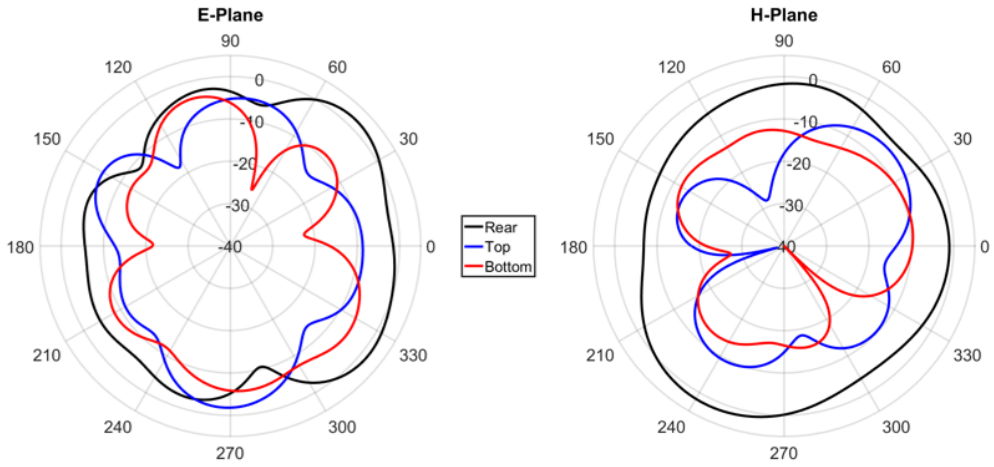

Figure 4.17: Radiation pattern E-Planes (left) and H-Planes (right) of 20 MHz nominal CFDA conformally attached to IRIS aircraft in top, bottom, and rear locations showing impact of placement on antenna functionality

Unlike the narrowband variation, the wideband CFDA does not have a definitively better radiation pattern in the E-Plane between the three positions. Figure 4.20 shows that all three variations have comparable average realized gain and the top variation actually has the highest degree of quasi-isotropy. The rear variation does however stand out when compared to the other two variations in the H-Plane. It has the highest realized gain for over 80% of the plane, only surpassed by the

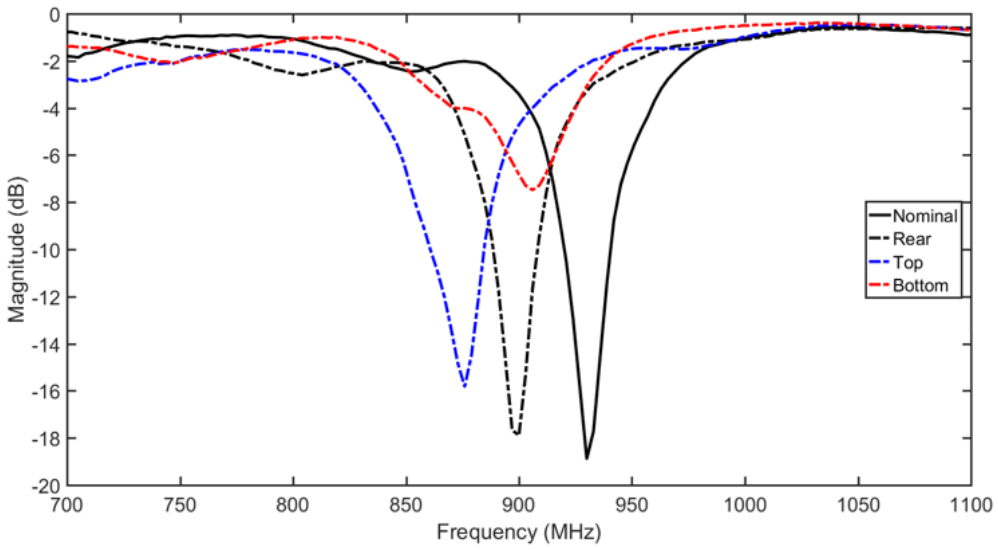

Figure 4.18: Insertion loss of nominal 20 MHz bandwidth CFDA conformally attached to IRIS aircraft in top, bottom, and rear locations showing impact of placement on antenna functionality

top variation which is substantially less quasi-isotropic. While not as much of a standout as an optimal choice, the rear once again shows the best overall radiation characteristics for these applications with the top position as a reasonable alternative.

The wideband CFDA exhibited substantially more response to craft loading effects on the insertion loss than the narrowband variation. The top variation was rendered virtually unusable with a minimum insertion loss greater than -7 dB, as depicted in Figure 4.21. The bottom and rear variations exhibit operating frequency shifts that are nearly identical, but the insertion loss of the bottom variation is also substantially hindered. The -10 dB bandwidth of the bottom variation is reduced to approximately 25 MHz while the rear variation retains its original 80 MHz bandwidth and the insertion loss hovers at quite nearly -10 dB for another 100 MHz upwards. Thus the rear variation again performs preferably of the positions tested for these applications, although with substantially more variation than that of the

narrowband design.

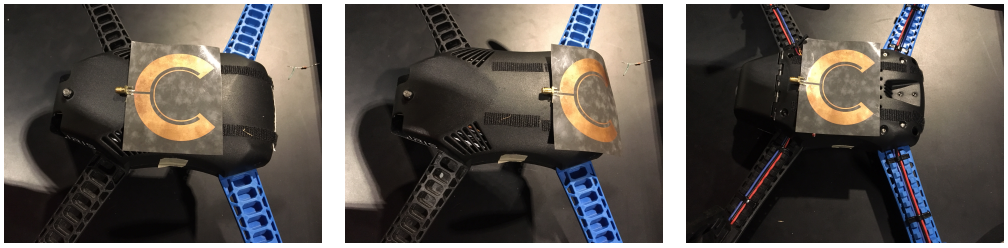

Figure 4.19: Conformally mounted 20MHz bandwidth CFDA variation in the top (left), rear (middle), and bottom (right) positions as mentioned

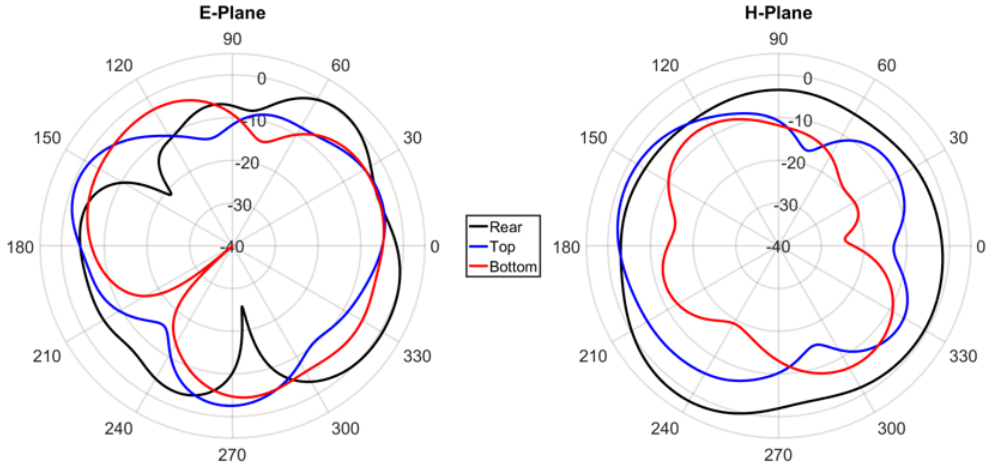

Figure 4.20: Radiation pattern E-Planes (left) and H-Planes (right) of 80 MHz nominal CFDA conformally attached to IRIS aircraft in top, bottom, and rear locations showing impact of placement on antenna functionality

4.6 Modifications for Conductive Backing

With the demonstrated effects of craft internals affecting the performance of the CFDA, an investigation into the use of a ground plane for the purpose of isolation was pursued. Generally, dipole-like structures suffer significant reduction in radiation efficiency when placed at small fractions of a wavelength away from a ground

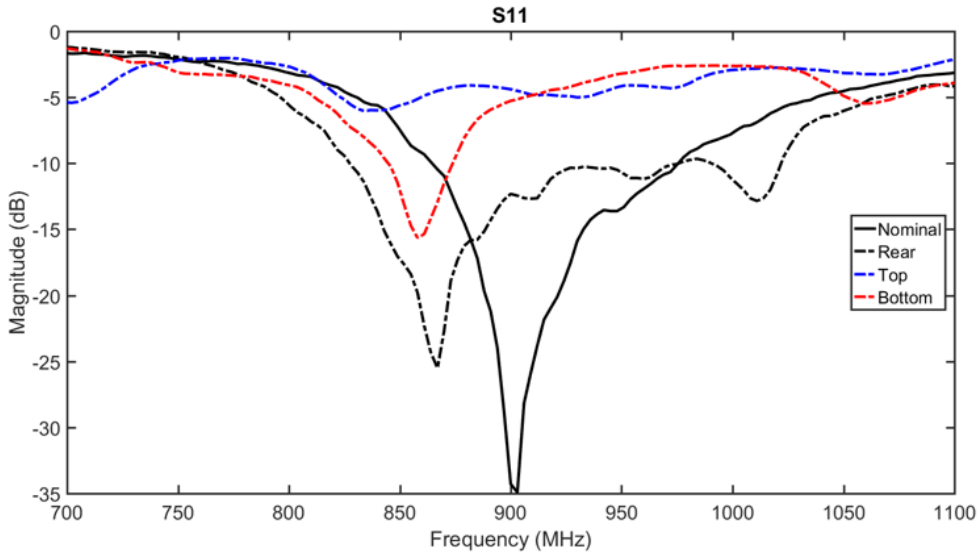

Figure 4.21: Insertion loss of nominal 20 MHz bandwidth CFDA conformally attached to IRIS aircraft in top, bottom, and rear locations showing impact of placement on antenna functionality

plane, but previous work has shown that this is at least partially a correctable result of substantially reduced impedance [24]. However, a more substantial change in impedance is necessary from those previously discussed thus far to maintain a conformal structure within the space constraints of a SUAS. A maximal thickness of 3mm, the thickness of the substrate and Velcro, is used to maintain consistency with the packages sizes used throughout this work thus far. This constrains the electrical distance from the ground plane to $\lambda/100$ or less at the telemetry frequency of 915 MHz.

Using another instance of classical folded dipole impedance theory, the antenna can be split into more than two concentric lines beyond the nominal two to further raise the impedance. When lines are kept equivalent in size, a special case of this methodology dictates the impedance scaling factor is N^2, where is N the number of lines [23]. As the number of lines increases in the CFDA however, this special case is not precisely upheld as the lines progressively diverge in electrical length

and are thus not equivalent in another manner. The result of increasingly divergent line length in simulation is the contraction of the frequency span between the parallel resonances of the antenna. The square factor can still be roughly applied to the general number of lines but will not converge in one of the extrema, as depicted in Figure 4.22. Additionally, the bandwidth is substantially reduced due to the frequency compression of the reactance curve between the resonances. The desired number of lines needed to step up from a nominal CFDA design to a higher impedance in this manner is

$$N = \sqrt{\frac{4 * R}{R_0}}; \tag{4.4}$$

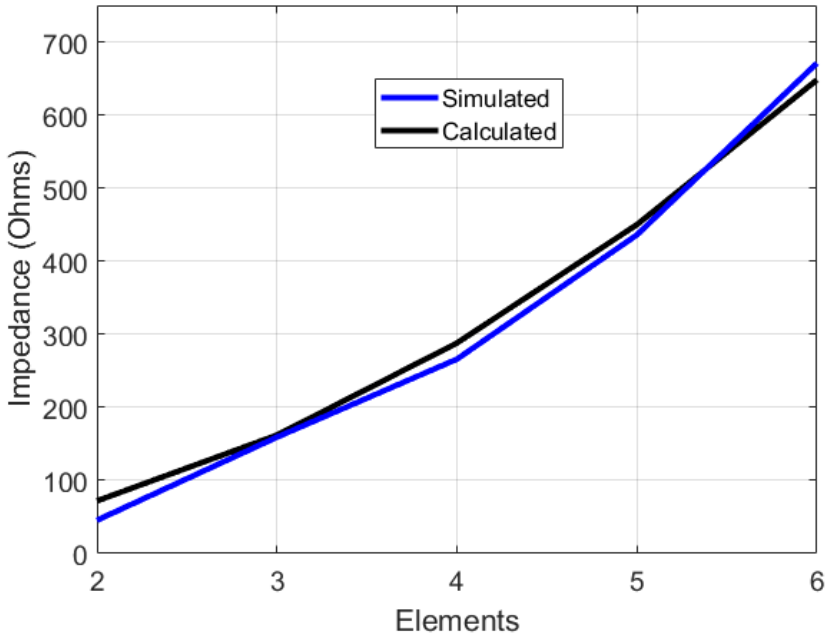

Figure 4.22: Comparison of CFDA impedance variations projected by conventional folded dipole impedance scaling to simulations, resulting from adding additional radiating elements to the folded dipole structure

To minimize the effect of size imbalance, trace widths and spacing were re-

stricted to the smallest recommended size for the in-house lithography process of 0.5mm. A standard 2-line CFDA with these parameters and 180° of curvature resulted in a simulated input impedance of 4.5 Ω at 915 MHz. Equation 4.4 indicates that 7 lines are needed in a CFDA to step up the impedance to approximately 50 Ω. The 7-line CFDA shown in Figure 4.23 was simulated in HFSS with both large and small ground planes and, as with the 2 to 6 line variations, exhibited a very small bandwidth at 3 MHz. With a ground plane restricted to the size of the radiating element, the efficiency of the antenna was 30% although with considerable back-plane radiation indicating a lack of significant isolation. A full-wavelength ground plane centered on the element forced the antenna to exhibit minimal back-plane radiation but reduced the efficiency to 10.5%. Although the efficiencies are substantially higher than those of linear dipole structures at the same spacing, they still remain undesirably low and the combination with poor bandwidth and hemispherical radiation characteristics make them minimally useful for SUAS in their present state. The general investigation of antenna structures for conductively backed implementations is a topic of future work.

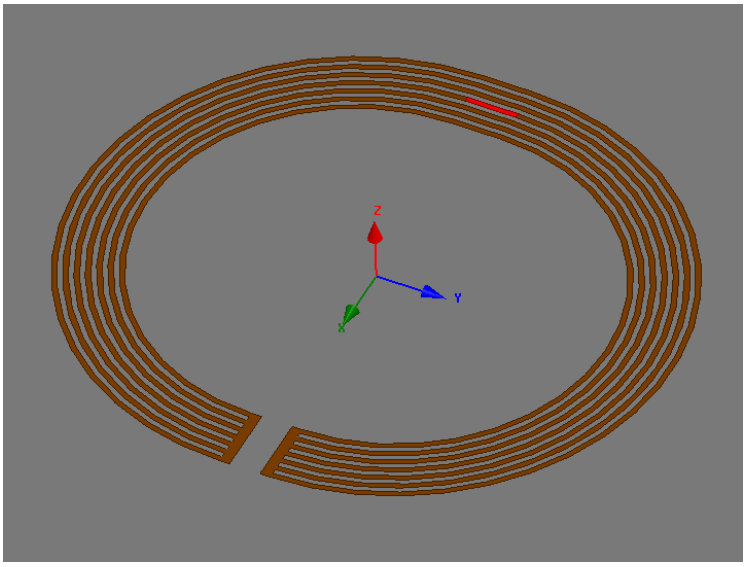

Figure 4.23: Close-up geometry of the 7-line CFDA implemented on a full-wavelength square 10 mil substrate with a ground plane 3mm below

4.7 Conclusions

The curved folded dipole antenna achieved both the implementation simplicity and quasi-isotropic pattern desired for this work. Although the radiation pattern was volatile regarding conformal placement, it was still void of any deep radiation nulls characteristic of dipoles of the impedance modified loops previously discussed. A radiation pattern prediction model was generated from modeling the structure as a series of current-scaled infinitesimal dipoles. This model showed excellent convergence with both simulated and measured results for the angles of curvature examined. The CFDA exhibited performance flexibility in radiation pattern, impedance, and bandwidth. The flexibility of each parameter was modeled using the current model and extensions of conventional folded dipoles theory that were shown to numerically hold for the curved structure.

Both fabricated variations of the antenna, with bandwidths of 20 MHz and 80

MHz, showed an ability to conform to the craft with an optimal placement and retain at least the minimum desired specifications for the onboard telemetry module. The 20 MHz variation retained both its radiation pattern and insertion loss characteristic better than its 80 MHz counterpart. The 80 MHz variation saw the beginnings of radiation nulls in its E-Plane and exhibited a great deal of volatility in its insertion loss when conformed. Nevertheless, the performance flexibility is simply an added benefit to the already achieved quasi-isotropy and simplicity of implementation.

Chapter 5

Flight Measurements

5.1 Introduction and Goals

In situ flight testing was necessary to gauge the ability of the antennas to tangibly improve communications in SUAS operations. Variations of the loaded loop antennas and CFDA discussed herein were measured on crafts in tandem with basiline measurements performed using the stock antennas for each platform. The main goal of these tests was to assess how the antennas performed when mounted to a non-ideal structure with potentially large sources of interference and loading including the multiple transmission systems, large batteries, and populated PCBs. Nominal measurements focus on the received signal strength indicator (RSSI) values and the bit error rate (BER) recorded between the base station and on-board telemetry. Where possible, RSSI has been converted to dBm for a more straightforward metric and is generally linearly correlated with dBm [25]. Measured results show that BER is a relatively volatile metric in the range of power levels where communications begin to falter, so more telling metrics such as phase noise and modulation error are being pursued with software defined radio (SDR) modules as a means to give a more definitive representation of the communication performance.

5.2 Fixed Wing Flight Tests

A 50 Ω variation of the impedance modified loop antenna was tested conformally mounted in flight, as shown in in Figure 5.1, to a styrofoam-bodied fixed-wing craft operated by a crew from the University of Kentucky. The aircraft normally employs a diversity of rubber duck antennas and communicates through the link providing the largest power throughput at regular transmit intervals. In these tests, the two telemetry rubber duck antennas were removed and the module was wired with 30cm cables to two perpendicularly mounted impedance modified loop antennas.

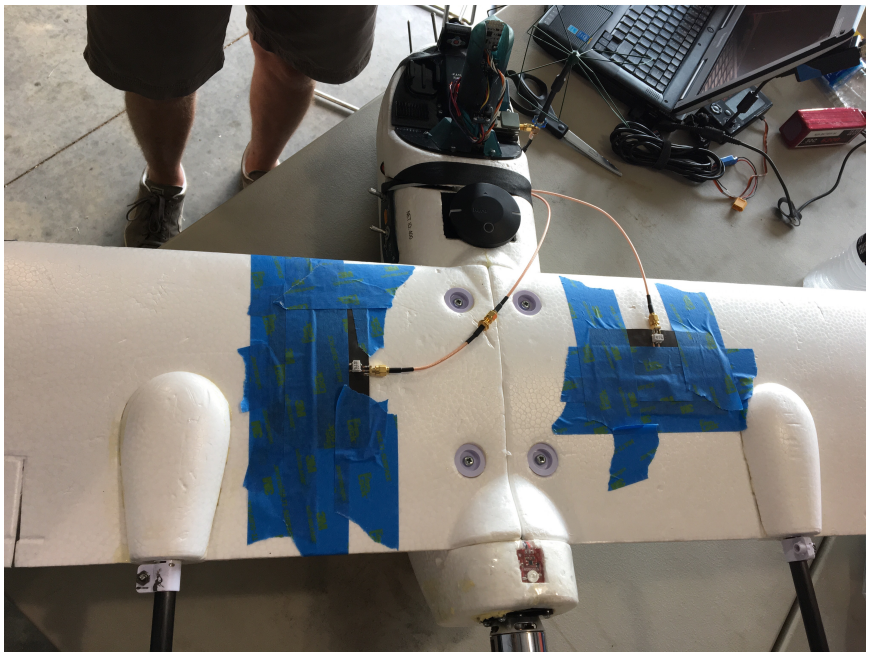

Figure 5.1: Perpendicular conformal implementation of loaded loop antennas adhered to University of Kentucky styrofoam fixed-wing aircraft with masking tape

The recorded RSSI and BER for both a flight with and without the loaded loop are shown in in Table 5.1. The craft performed maneuvers at both a low altitude and lateral distance (short-range) and a large altitude and lateral distance (long-range). For both the long-range and short-range flights, the loaded loop antennas

performed almost equivalently, but slightly better, in both average RSSI and BER than the variety of rubber duck antennas previously installed in the craft. This suggests that the loaded loops could be a viable replacement for the onboard rubber duck antennas at 915 MHz. The advantage of doing so on such a platform is the ability to conformally mount, or potentially integrate within the wind structure, such an antenna both freeing up space in the fuselage and distancing the antenna from loading or interference from otherwise nearby components of the flight system. As styrofoam has a typical dielectric constant very close to that of air, there can be large flexibility in placement and integration with favorable consistency to expected results in air.

Table 5.1: In-flight performance results for the 50Ω loaded loop antenna on the University of Kentucky fixed-wing aircraft

Antenna	Short-Range Mean RSSI	Long-Range Mean RSSI	Short-Range BER	Long-Range BER
Loaded Loop (with chip balun)	201.25	143.59	1.25×10^{-5}	3.60×10^{-5}
Rubber Duck (normal mode helix)	192.72	134.28	2.09×10^{-5}	3.83×10^{-5}

5.3 Quadrotor Tests

The primary test platform for the variety of antennas discussed herein is the IRIS family of quadrotor SUAS. Antennas were tested with the 915 MHz telemetry link both conformally mounted and attached protruding from the antenna rear antenna port, as depicted in Figure 5.2. The rubber duck antenna included with the IRIS and used for testing is of the coiled whip variety, mounted only in the standard protruding position, and has a radiation pattern depicted in Figure 2.1. The radiation patterns for the nominal CFDA and impedance modified loop antenna were measured with conformal placement on the rear of the craft as was determined to be

optimal for the IRIS craft previously of those tested. Since the rear placement involves slight conformation at an angle about the rear of the craft with the feed-side portion of the antenna nearly planar, the E and H plane comparisons are referenced as through the antenna was laid flat upon the top of the craft. The CFDA and loop radiation patterns, depicted in Figure 5.3 and Figure 5.4 respectively, show that there is substantial variation from the simulated and measured patterns in air. This variation is largely due to the conglomeration of electronics in the fuselage that undesirably load the antennas and scatter the radiation. The conformal radiation pattern shown is that corresponding to rear placement previously determined to be optimal of the positions tested.

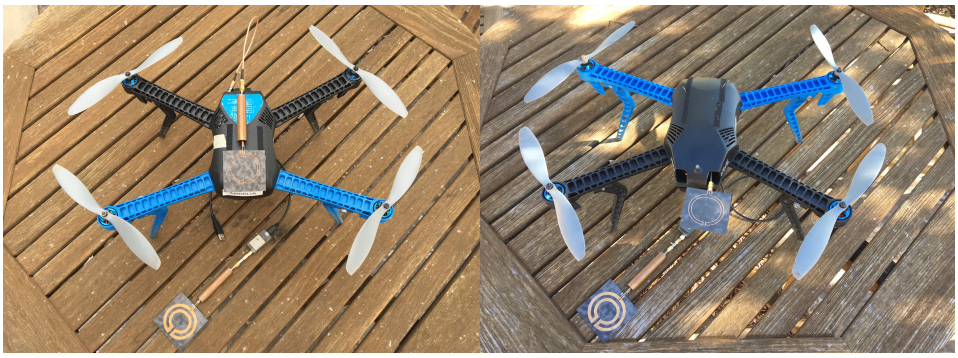

Figure 5.2: Quadrotor test configuration for antennas in both conformal (left) and non-conformal (right) configurations on the IRIS aircraft

5.3.1 Power Transfer and BER

The telemetry system onboard the IRIS directly supplied RSSI and received error rate information. The telemetry link operates over a maximal bandwidth of 902 MHz to 928 MHz using Gaussian Minimum Shift Keying (GMSK) and implements Golay encoding for error correction. This method of enconding represents each 12 bits of information with 24 bits of data, allowing the system to detect errors

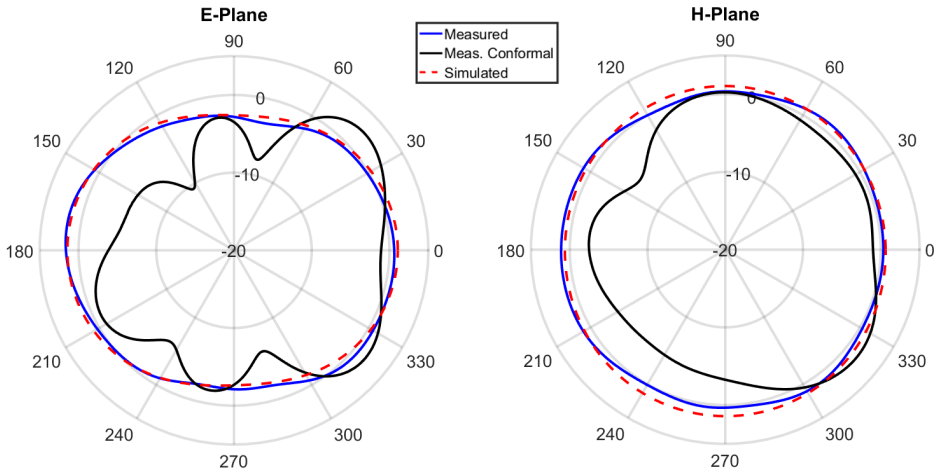

Figure 5.3: CFDA radiation pattern measurements depicting substantial variation from simulation and air measurement when adhered to craft with 3mm thick Velcro

of up to 7 bits and correct sequences containing 3 or fewer errors [25]. Thus the uncorrected error rate for the telelmetry link is expected to climb substantially when the mean number of errors per 12-bit packet exceeds 3. The RSSI on the Si1000 RF microcontroller in the 3DR telemetry module scales approximately linearly with the received dBm power, minus an offset corresponding to the transceiver sensitivity [25]. The sensitivity of the module used is -127 dBm. Given an output RSSI level, the received power is

$$dBm = (RSSI/1.9) - 127 \tag{5.1}$$

To generate a set of baseline communication metrics for the IRIS system, the craft was set to perform three cycles vertically ascending to and descending from 100 meters at approximately 10 meters from the base station with the antennas mounted extended from the craft body, as shown in Figure 5.5. Baseline results were generated for the IRIS standard rubber duck antenna, the impedance modified loop, and the nominal CFDA with 20 MHz of bandwidth. Figure 5.2 depicts the approximate communication metrics generated through the initial antenna testing with the IRIS

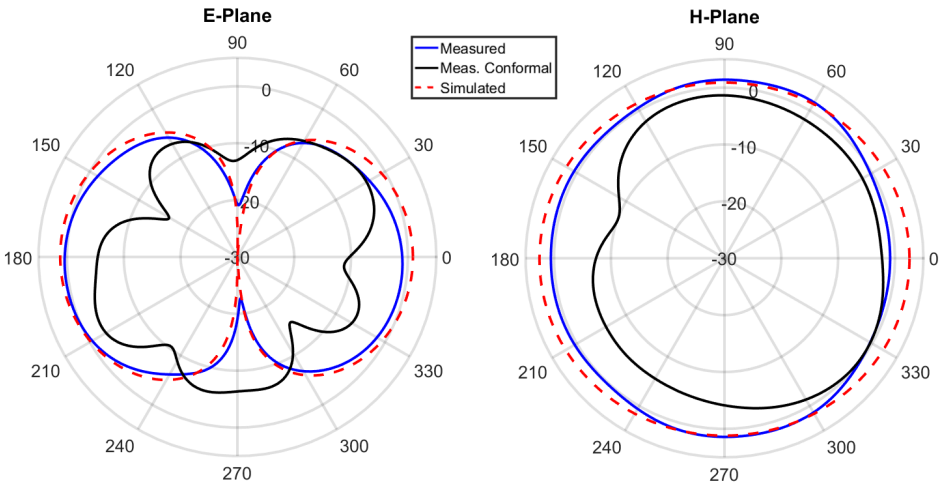

Figure 5.4: Impedance modified loop radiation pattern measurements depicting substantial variation from simulation and air measurement when adhered to craft with 3mm thick Velcro

aircraft, including the RSSI and resulting calculated dBm as well as both the post-correction and overall bit error rates. In both power transfer and total bit error rate, both of the novel antenna structures were shown to perform at least ten times better than the included rubber duck antenna. The impedance modified loop provides a further improvement over the CFDA in power transfer and bit error rate of approximately 3.5 dBm and a factor of two, respectively. The higher directivity of the loop in the vertical direction and higher bandwidth compared to the CFDA suggests this is a valid result for a flight essentially directly overhead, but would not hold if the craft maneuvered at range and communicated in a direction in the vicinity of its radiation nulls.

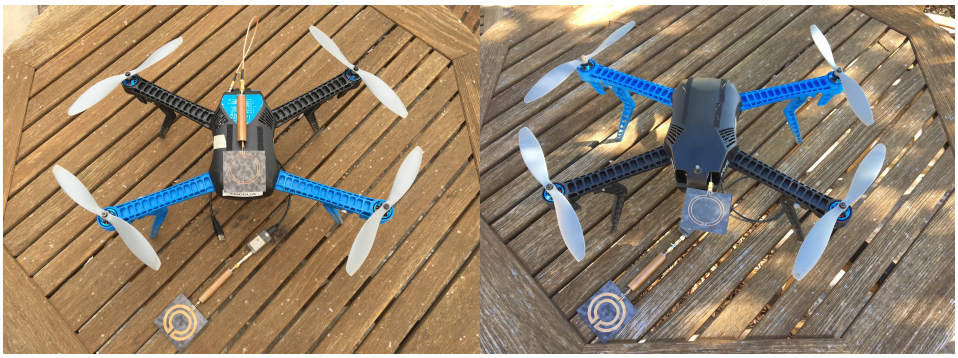

Figure 5.5: Example antenna configurations for base station telemetry module and for IRIS aircraft with both conformal (left) and non-conformal (right) positioning on the aircraft

Table 5.2: Communication metrics generated from telemetry data from flying the IRIS craft to 100 meters with antennas positioned standalone from the airframe

Antenna	Mean RSSI	Mean dBm Received	Uncorrected Bit Error Rate	Total Bit Error Rate
Rubber Duck	108.05	-70.13	12.8×10^{-7}	15.0×10^{-7}
Impedance Modified Loop	140.45	-53.08	0.64×10^{-7}	1.07×10^{-7}
Curved Folded Dipole (20 MHz)	131.63	-57.72	1.41×10^{-7}	1.50×10^{-7}

Vertical profiles with a comparably short horizontal approach were once again used to asses the communication abilities at extended range and conformally mounted to the surface of the craft with 3 mm high Velcro strips. The primary test featured the IRIS performing a single ascent to and descent from 300 meters at a range of 50 meters from the ground station. In addition to the three antennas used for baseline testing, the wideband variation of the CFDA with 80 MHz of bandwidth was added to see potential impacts of limited bandwidth on the nominal CFDA and the recession towards a linear dipole radiation pattern incurred by the bandwidth exten-

sion procedure previously discussed. The performance metrics in Table 5.3 show largely the same relationship as the baseline testing, with all three novel antennas outperforming the rubber duck antenna. The impedance modified loop and both CFDA variations exhibited a total bit error rate of at least twenty times less and power levels 8.5 to 15 dBm higher than those of the rubber duck antenna. In these tests, however, the impedance modified loop was actually shown to perform less effectively compared to the CFDA variations. Since the majority of the errors for the impedance modified loop occur on the 50m lateral approach path from the base station when the null is most directly pointed at the base station for the flight, it is theorized that the communication is indeed hindered when maneuvering in such a direction but flights that better profile the whole of the antenna relative to the ground station need to be performed to fully validate this theory. Additionally, the nominal CFDA was outperformed in power received and total bit error rate by the wideband CFDA by 1 dBm and 60 %, respectively. The wideband CFDA had decreased insertion loss towards its respective band edges as the nominal CFDA did not cover the entirety of the 26MHz operating band and, as the investigation of placement sensitivity suggests, it should not have been as volatile in resulting performance over the operating band due to the loading effects from conformal mounting near craft internals.

Table 5.3: Communication metrics generated from telemetry data from flying the IRIS craft to 300 meters with antennas positioned conformal to the structure, wrapping slightly about the top of the front end

Antenna	Mean RSSI	Mean dBm Received	Uncorrected Bit Error Rate	Total Bit Error Rate
Rubber Duck	60.34	-95.24	14.2×10^{-7}	78.2×10^{-7}
Impedance Modified Loop	77.61	-86.15	1.34×10^{-7}	3.12×10^{-7}
Curved Folded Dipole (20 MHz bandwidth)	88.95	-80.18	1.12×10^{-7}	1.80×10^{-7}
Curved Folded Dipole (80 MHz bandwidth)	91.15	-79.03	0.86×10^{-7}	1.07×10^{-7}

5.3.2 Multi-Metric Assessment with SDR

On-board radio performance metrics from the integrated communications system provide meaningful baseline results, but it is apparent in the bit error rate measurements that the results are highly volatile with changing levels of power transfer. This volatility is inherently linked in part to the error correction encoding which has set limits in practical implementations. For the IRIS the corresponding limits are 3 errors and 7 errors for correction and detection, respectively. Such results could thus be highly skewed based on available power from the transmit module and momentary periods of complete signal loss. Thus, software defined radio modules were added to the test regiment to include a capability for more stable test metrics such as modulation noise and signal to noise ratios. The capability for designation of modulation schemes and error correction mechanisms additionally allows for the extraction of such metrics for the most basic of communication chains and those

with more sophisticated features such as error correction encoding as is present within the IRIS craft's communication system. These metrics are still linked to the nominal power used but tend to break down at the point where the SNR approaches one as opposed to a point in the operating region of the receiver in the case of BER on the IRIS.

5.3.3 Conclusions

Simulations suggested that as the rubber duck included with the craft was both lossy and plagued by a poor radiation pattern with multiple radiation minima, the novel impedance modified loops and CFDa variations should allow the telemetry to link more effectively. In all tests performed, the quantifiable results from the telemetry link confirmed what the simulations suggested. The CFDA and impedance modified loop antennas both improved the overall communication link and provided both better power transfer and a lower resulting error rate.

Nominal overhead testing as well as flights on the fixed wing craft showed that the impedance modified loops outperformed the rubber ducks in all metrics tested. As they are slightly more directive in free space, they also outperformed the CFDA variations in direct overhead testing. Both the CFDA and impedance modified loops provided at least a 12 dBm increase in power transferred and reductions in errors of 88% and 92% respectively. Conformal testing however seemed to favor the CFDA variations. As the loops suffer a worse radiation pattern degradation as a whole, the 20 MHz CFDA largely retains its pattern and the 80 MHz CFDA is only degraded substantially in its acquired null directions. Additionally, since the 20 MHz variation is operating at or near its band edges, it suffers some losses that allow the 80 MHz variation to overtake it.

Through multiple flights and varying configurations, the impedance modified loops and CFDA variations were shown to indisputably improve the overall communications of the craft. The significant reduction in errors directly translates to less loss of real-time meteorological measurements on the intended vehicles. When extended to 2.4 GHz implementations, they also have the potential to heavily reduce the likelihood of critical communications losses and dangerous events such as flyaways.

Chapter 6

Conclusions and Future Work

6.1 Conclusions

Rubber duck antennas remain the most ubiquitous antenna structure for SUAS applications. They, in conjunction with the newly popularized cloverleaf antennas, share the drawback of deep radiation nulls. Additionally, the coiled whip variety of rubber ducks, implemented for electrical size reduction, suffer losses and reduced radiation efficiency. Neither structure is conformal, and cloverleafs require significant volumes to implement relative to their electrical size. A brief survey of conformal and quasi-isotropic radiators showed that both properties have been well established for individual use but few antennas utilize both. Even fewer can be implemented conformally within the size constraints of SUAS. The theory of othogonal currents for quasi-isotropic pattern production and in particular, a split folded dipole [13], provide a pathway for further designs.

Pursuit of performance-flexible conformal antennas first led to investigation of impedance modified loop antennas. Simulations in HFSS showed that the impedance may be varied all the way to 0 Ω from the nominal loop impedance, giving the design a great deal of flexibility. A numerical model was developed for the resulting impedance given a percentage of the interior of the loop filled by a metal patch.

This was shown to have an accuracy of 1 Ω for the specific design discussed and within 7.5 Ω for generalized rectangular loops of arbitrary dimensions. The equation was solved for the patch to radiator distance such that approximately matched loops can be designed numerically with ease and without the necessity of a full-wave solver. These loops were then shown to perform comparably to an ideal half-wave dipole and be able to conform with minimal interference when strategically placed on an SUAS. At a full wave in circumference, the impedance modified loops push the limits of practical size for SUAS applications in their basic configuration. Thus, methods for miniaturization were briefly explored to further solidify them as a baseline solution. While they may not provide a quasi-isotropic pattern, they are an immediate improvement over lossy rubber duck structures and add the desired trait of conformality. Additional investigation of size reduction and self-contained loading techniques is needed for this class of antennas. Achieve these properties would make the class more universally applicable to dielectric-bodied SUAS.

As an initial step into the genre of isotropic radiators, a modified version of crossed dipoles was investigated. Previously literature suggested crossed dipoles would generate sufficiently quasi-isotropic radiation for SUAS applications, so an investigation of their ability to thus be reduced in size and conform was amply merited. Using the idea of orthogonal distribution of currents and with the desire for size reduction, each element was bent halfway along its length perpendicularly. This, in conjunction with the addition of small meander line end loads, reduced the effective area required for the crossed dipole structure by over 60%. Surface-level simulations also indicated that crossed dipole structures can achieve a 90 degree radius of curvature with minimal effects on their performance, so long as the elements are symmetric. Ultimately the antenna structure was held back by practical implementation challenges. Requiring two seperate ports with a 90 degree phase shift

between them, as well as a impedance transform to match to 50 Ω when connected in parallel, made them less practical as a general purpose solution. Revisiting these antennas to an attempt to raise the operating impedance and implement a small hybrid coupler for the phase shifting mechanism could also prove the viability of these antennas for SUAS applications.

Returning to the theory of the split folded dipole [13], however, led to the creation of the curved folded dipole antenna. Using the same theory of distributed currents, a quasi-isotropic radiator was created using a folded dipole as the fundamental structure. By curving it in-plane, the impedance can be matched to 50 Ω without transformation and the normalized radiation pattern minima can be brought up to at least -3.5 dB. A numerical model was developed to approximate the radiation pattern based on the angle of curvature by approximating the radiation of the antenna as current-weighted segments of the dipole mode wrapped circularly. This model showed good convergence with both the simulated and measured results. Portions of conventional folded dipole theory related to impedance modification were investigated and shown to hold for this structure given considerations for the altered geometry. Using modified versions of the conventional equations, the structure was shown to be impedance, pattern, and bandwidth flexible. The modified impedance predictive equations showed excellent consistency with simulations despite a divergence in geometry from a nominal folded dipole. An approximate model for the impedance and curvature relationship is in development with an aim of rapid prototyping as with the impedance modified loops. This would provide another numerically designable antenna given the other performance relationships already established herein. The CFDA was also tested conformally to establish what effect a craft may have upon its performance. When kept out of the vicinity of large electronics, it was shown to perform similarly in insertion loss characteristic and ra-

diation pattern, albeit with a noticeable frequency shift that could be pre-accounted for. The wider bandwidth version of the CFDA retained a -10 dB insertion loss over the desired band but also showed much more volatility in radiation pattern adn overall insertion loss characteristics. This volatility is hypothesized to arise from the uneven distribution of current on the elements that is used to develop the wider bandwidth, but the relationship needs further characterization. True optimization of the antenna structure for a given parameter as well as a fully characterized model to accomplish this end is the primary goal of future work. As the antenna nominally achieves the small conformal properties desired, this would make it the ideal candidate for an easily usable structure for the scientific community at large.

Finally, the impedance modified loops and CFDA variations were tested against the rubber duck antennas provided with an IRIS quadrotor SUAS to assess the tangible changes in communication efficiency they may provide. In all tests, use of the impedance modified loops and CFDA variations corresponded to an increase in power transfer of at least 9 dB or and decreases in bit error rates of 85% or more. In non-conformal testing, the impedance modified loops slightly outperformed the nominal CFDA as they ideally had higher realized gains in the directions tested. However, they were shown to suffer significant E-plane radiation pattern degradation in conformal radiation pattern testing. This resulted in both CFDA variations outperforming the loops in power transfer and BER when tested conformally placed on the rear section of the craft. Additionally the 80 MHz bandwidth variation showed improvement over the nominal 20 MHz bandwidth variation, likely due to the impedance mismatch from conformation and resulting higher insertion loss at the band edges. Further optimization of placement, conformal shape, and body material are necessary as future work to definitively characterize these structures as well.

The impedance modified loops have been shown to provide improvements in every metric considered over the stock rubber duck antennas for the IRIS and additionally add the desired trait of conformality. A numerical model will allow for rapid prototyping and adjustment of these antennas structures in the future. The curved folded dipole was shown to be a further general solution improvement over the impedance modified loops as it adds quasi-isotropy. Its highly flexible performance parameters, which have been partially numerically modeled as well, allow for customization to a given application with minor geometric alterations. Finally, both antenna classes are shown to significantly improve the performance of the communication link when either extended from or conformally adhered to the craft in the optimal position.

References

[1] Y. Chen and C. F. Wang, "Electrically small uav antenna design using characteristic modes", *IEEE Transactions on Antennas and Propagation*, vol. 62, no. 2, pp. 535–545, Feb. 2014, ISSN: 0018-926X. DOI: 10.1109/TAP.2013.2289999.

[2] Z. Q. Liu, Y. S. Zhang, Z. Qian, Z. P. Han, and W. Ni, "A novel broad beamwidth conformal antenna on unmanned aerial vehicle", *IEEE Antennas and Wireless Propagation Letters*, vol. 11, pp. 196–199, 2012, ISSN: 1536-1225. DOI: 10.1109/LAWP.2012.2187321.

[3] K. Obeidat, R. G. Rojas, and B. Raines, "Design of antenna conformal to v-shaped tail of uav based on the method of characteristic modes", in *2009 3rd European Conference on Antennas and Propagation*, Mar. 2009, pp. 2493–2496.

[4] H. Mathis, "A short proof that an isotropic antenna is impossible", *Proc IRE*, vol. 39, no. 8, p. 970, 1951.

[5] ——, "On isotropic antennas", *Proc IRE*, vol. 42, p. 1810, 1954.

[6] W. Saunders, "On the unity gain antenna", *Electromagnetic Theory and antennas*, p. 1125, 1963.

[7] W. Scott and K. Hoo, "A theorem on the polarization of null-free antennas", in *1965 Antennas and Propagation Society International Symposium*, vol. 3, Aug. 1965, pp. 282–282. DOI: 10.1109/APS.1965.1150296.

[8] G. Deschamps, J. Dyson, and P. Mast, "Two-port isotropic radiator for unpolarized waves", *IEEE Transactions on Antennas and Propagation*, vol. 17, no. 6, pp. 809–810, Nov. 1969, ISSN: 0018-926X. DOI: 10.1109/TAP.1969.1139543.

[9] S. R. Ganti and Y. Kim, "Design of low-cost on-board auto-tracking antenna for small uas", in *2015 12th International Conference on Information Tech-*

nology - New Generations, Apr. 2015, pp. 273–279. DOI: 10.1109/ITNG.2015.50.

[10] R. Mellen and C. Milner, "The skew-planar wheel antenna", *QST*, Nov. 1963.

[11] ARRL, "A circular antenna for u.h.f.", *QST*, Nov. 1942.

[12] P. H. Smith, ""cloverleaf" antenna for f.m. broadcasting", *Proceedings of the IRE*, vol. 35, no. 12, pp. 1556–1563, Dec. 1947, ISSN: 0096-8390. DOI: 10.1109/JRPROC.1947.230912.

[13] E. da S. Pires, G. Fontgalland, R. M. do Valle, G. F. Aragao, W. R. N. Santos, and T. P. Vuong, "Proposal of a new compact isotropic antenna", in *2006 IEEE International Symposium on Electromagnetic Compatibility, 2006. EMC 2006.*, vol. 1, Aug. 2006, pp. 125–128.

[14] Z. Su, F. A. Ghaffar, M. F. Farooqui, R. M. Bilal, and A. Shamim, "Design methodology of single-feed compact near-isotropic antenna design", in *2017 11th European Conference on Antennas and Propagation (EUCAP)*, Mar. 2017, pp. 3559–3562.

[15] M. F. Farooqui and A. Shamim, "A 3d printed near-isotropic antenna for wireless sensor networks", in *2016 International Symposium on Antennas and Propagation (ISAP)*, Oct. 2016, pp. 94–95.

[16] J. H. Kim, H. Kim, and S. Nam, "Design of a compact quasi-isotropic antenna for rf energy harvesting", in *2017 IEEE Wireless Power Transfer Conference (WPTC)*, May 2017, pp. 1–3.

[17] J. Kim, M. Ngatoshi, and H. Morishita, "Fundamental characteristics of a strip folded dipole antenna with a feed line having a hemispherical structure", in *2010 IEEE Antennas and Propagation Society International Symposium*, Jul. 2010, pp. 1–4. DOI: 10.1109/APS.2010.5561717.

[18] Z. Zhang, X. Gao, W. Chen, Z. Feng, and M. F. Iskander, "Study of conformal switchable antenna system on cylindrical surface for isotropic coverage", *IEEE Transactions on Antennas and Propagation*, vol. 59, no. 3, pp. 776–783, Mar. 2011, ISSN: 0018-926X.

[19] HMGCC, *Loop antennas*, Allerton Antenna Applications Symposium, 2015.

[20] M. F. Bolster, "A new type of circular polarizer using crossed dipoles", *IRE Transactions on Microwave Theory and Techniques*, vol. 9, no. 5, pp. 385–388, Sep. 1961, ISSN: 0097-2002.

[21] Y. Saita, N. Kagiyama, T. Ito, and H. Morishita, "Fundamental characteristics of a circular combined folded dipole antenna with a feed line", in *2014 IEEE Antennas and Propagation Society International Symposium (APSURSI)*, Jul. 2014, pp. 1011–1012. DOI: 10.1109/APS.2014.6904833.

[22] T. Yamano, J. Itoh, K. Yongho, A. Kajitani, and H. Morishita, "Fundamental characteristics of planar folded dipole antenna with a feed line", in *2008 IEEE Antennas and Propagation Society International Symposium*, Jul. 2008, pp. 1–4. DOI: 10.1109/APS.2008.4618938.

[23] K. Bakshi, *Antenna And Wave Propagation*. Technical Publications, 2009, ISBN: 9788184312119.

[24] Best, "Improving the performance properties of a dipole element closely spaced to a pec ground plane", *IEEE Antennas and Wireless Propagation Letters*, vol. 3, pp. 359–363, 2004, ISSN: 1536-1225. DOI: 10.1109/LAWP.2004.840722.

[25] ArduPilot, *Sik radio advanced configuration*, http://ardupilot.org/copter/docs/common-3dr-radio-advanced-configuration-and-technical-information.html, Accessed: 2017-08-18.

[26] D. Pozar, *Microwave Engineering*, 4th ed. Hoboken, NJ: John Wiley & Sons, 2012.

[27] C. Balanis, *Antenna Theory: Analysis and Design*, 3rd ed. Hoboken, NJ: John Wiley & Sons, 2005.

[28] ——, *Advanced Engineering Electromagnetics*, 2nd ed. Hoboken, NJ: John Wiley & Sons, 2012.